Int. J. Multiphase Flow Vol. 16, No. 5, pp. 761–788, 1990
Printed in Great Britain.

0301-9322/90 $3.00 + 0.00

MHD EFFECT ON NaK–NITROGEN TWO-PHASE FLOW AND HEAT TRANSFER IN A VERTICAL ROUND TUBE

A. SERIZAWA, T. IDA, O. TAKAHASHI and I. MICHIYOSHI
Department of Nuclear Engineering, Kyoto University, Yoshida, Sakyo, Kyoto 606, Japan

(*Received* 25 *January* 1989; *in revised form* 1 *April* 1990)

Abstract—The magnetohydrodynamic (MHD) effect on NaK–nitrogen two-phase flow and heat transfer has been experimentally studied in a vertical round tube in a transverse magnetic field. This study covered a wide range of two-phase flow patterns from bubbly flow to annular/annular–dispersed flow, including flow pattern observation and measurements of phase distributions, liquid film behavior and heat transfer coefficients. MHD effects on local flow structures and heat transfer mechanisms have been discussed based on these measurements. It has been found that the application of a magnetic field brought about a significant asymmetric behavior both in two-phase flow structures and heat transfer. The angular dependence of heat transfer in annular/annular–dispersed flow is particularly stressed.

Key Words: liquid metal–gas flow, MHD effect, flow structures, heat transfer

1. INTRODUCTION

In recent years much attention has been directed toward studying liquid metal–gas two-phase mixture flows in relation to various energy conversion systems and injection metallurgy. In particular, a recently developed conceptual design for fusion reactors and liquid metal magneto-hydrodynamic (MHD) power generators demands accurate and reliable knowledge of the heat transfer and thermohydraulic mechanisms of liquid–gas two-phase flow in the presence of a magnetic field (e.g. Lielausis 1975; Petrick *et al.* 1977; Bender & Hoffman 1977; Branover *et al.* 1984).

Liquid metals show, in general, high heat transfer performances because of their higher thermal conductivity than ordinary fluids. It has therefore been the norm to use liquid metals as working fluids in compact-type high power density fusion reactor systems. However, liquid metal flow in a magnetic field suffers from a large magnetic pressure drop due to its large electrical conductivity. To overcome this problem, Bender & Hoffman (1977) proposed for the first time the use of liquid metal droplet–gas two-phase flow instead of liquid metal single-phase flow. However, no details of liquid metal–gas two-phase flow were studied by them.

The idea of using high-quality liquid metal–gas two-phase flow as a coolant flowing in a strong magnetic field is suggested on the basis of the following observations:

(1) The two-phase magnetic pressure drop is the same order of magnitude as the single-phase magnetic pressure drop due to the decrease in the effective electrical conductivity of the two-phase mixture, caused by the existence of the gas phase, though it is a strong function of the field strength with an increasing trend (Thome 1964). In other words, the two-phase magnetic pressure drop is substantially independent of the average field void fraction.
(2) It is well-accepted, as typically shown by Vershoor & Stemerding (1951), that, in ordinary fluid–gas two-phase flows, the heat transfer is greatly enhanced in annular or annular–dispersed flow.

Provided that the liquid metal–gas two-phase heat transfer performance follows the general trends observed in ordinary fluid–gas two-phase flows, mentioned above, the liquid metal–gas two-phase heat transfer could also be augmented in annular or annular–dispersed flow. In order to remove the same amount of heat, a smaller mass flow rate of liquid is therefore required for liquid metal–gas two-phase flow than for liquid metal single-phase flow, consequently causing a reduction in the magnetic pressure drop. It is thus understood that the application of high-quality liquid metal–gas two-phase flow to high efficiency heat transfer devices placed in a strong magnetic

field could have a potential advantage. However, it should be noted here that the above discussion is definitely based on the assumption that the heat transfer in liquid metal–gas two-phase flow, particularly in annular of annular–dispersed flow patterns, should be greater than that in liquid metal single-phase flow even in a magnetic field. This hypothesis has not been confirmed yet either experimentally or theoretically.

Referring to the comprehensive state-of-the-art review by Branover (1986a) of recent and currently ongoing work in the field of liquid metal MHD energy conversion systems (LMMHD), it is understood that the modern technology of LMMHD systems uses a gas–liquid two-phase mixture. Typical examples of these kinds are LMMHD systems performing an Ericson cycle and the OMACON-type system, which was designed and constructed by the Ben-Gurion University team. In the former system, both the gas expansion and gas compression are important thermodynamic processes taking place in gas–liquid two-phase flows. The kinetic energy of the liquid metal flow is converted to electric power via a near-isothermal gas expansion process. In the latter system, a vapor or gas is introduced as a thermodynamic working fluid into the mixer at the bottom of the upcomer channel, while a single-phase flow returns into the downcomer. The pressure difference that exists between the upcomer and downcomer due to the density difference is converted into electrical energy. Clarifying the mechanisms of two-phase pattern transition, phase distribution and flow structures in a magnetic field thus becomes important also.

Although a considerable number of works have been published so far, very little is known about the mechanisms involved in the heat transfer and local flow structures of liquid metal–gas two-phase flows. This is mainly due to a lack of detailed experimental data. For instance, recent works by Michiyoshi *et al.* (1977, 1986), Gherson & Lykoudis (1984) and Serizawa *et al.* (1986a) revealed the importance of flow regime observations and local turbulence measurement. This naturally incorporates the need to re-examine very carefully the experimental results reported previously in the literature.

The case of liquid metal–gas two-phase heat transfer is quite similar. It is generally believed that two-phase heat transfer in low quality is determined mainly by a balance between the decrease in the two-phase effective thermal conductivity and bubble agitation effects. The application of a magnetic field suppresses the turbulence motions of the liquid flow in the direction perpendicular to the field, thus leading to a deterioration in the heat transfer. This might be correct for a non-wetting liquid metal such as mercury, where bubbles tend to flow near heated walls (Michiyoshi *et al.* 1982). On the other hand, in NaK–gas flow, with a negligible amount of impurities in it which can wet solid surfaces, the effective thermal conductivity of the mixture in the near-wall region does not deteriorate so much, since bubbles are not collected on the wall (Serizawa & Kataoka 1987). Two-phase heat transfer is therefore enhanced due to bubble agitation in the bulk flow (Michiyoshi *et al.* 1986).

In annular–dispersed flow of liquid metal–gas two-phase systems, the magnetic field induces non-symmetric film flow structures on the heated walls, as will be shown later. This will cause either deterioration or enhancement of heat transfer, depending on the local flow conditions.

In a recent study by Inoue *et al.* (1987) using a lithium–helium annular–mist flow in a horizontal rectangular channel with a wall conductance ratio of 0.08, they correlated their own two-phase heat transfer data with the helium single-phase flow heat transfer coefficient. Some of their typical results are shown in figure 1, and indicate enhancement of heat transfer by application of two-phase annular–mist flow, as has been reported elsewhere for ordinary liquid–gas flow systems. They also observed that, when the magnetic field was varied up to 0.5 T, the ratio of the two-phase heat transfer coefficient with a magnetic field to that without a magnetic field increased almost proportionally with the magnetic field strength. Beyond 0.5 T, the results showed, at low and intermediate helium flows, nearly constant heat transfer ratios depending on the flow quality. For higher helium flow rates, the heat transfer ratio continued to increase with magnetic field strength. They hypothesized that these behaviors were related to the initiation of liquid droplet entrainment and deposition processes. It is, however, noted here that their measurement was restricted to the bottom wall of the rectangular channel, which is parallel to the field direction. By considering that, particularly in liquid metal–gas two-phase flow systems, the heat transfer depends very much on both the local flow structures and distributions of the liquid and gas phases (Michiyoshi *et al.* 1982, 1986; Serizawa *et al.* 1986a, b; Serizawa 1988; Ida *et al.* 1988), it appears difficult to draw

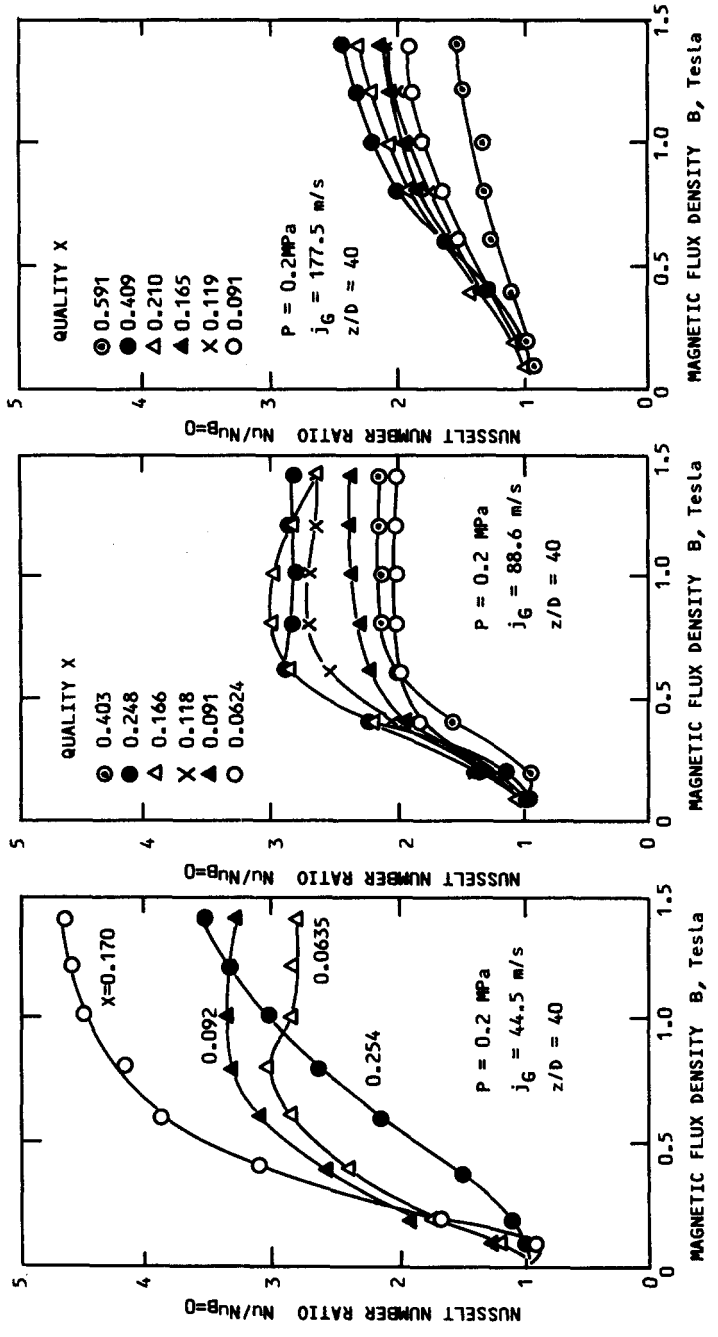

Figure 1. The MHD effect on heat transfer in helium–lithium annular–dispersed flow (Inoue *et al.* 1987).

generalized conclusions from Inoue's results alone. To the present authors' knowledge, the asymmetric flow distribution induced by the magnetic field has serious effects on the local heat transfer characteristics, as mentioned previously.

It is thus understood that the local flow structure and heat transfer mechanism are more closely linked in liquid metal–gas two-phase flow than in ordinary liquid–gas two-phase flow systems, since the thermal boundary layer thickness of a liquid metal two-phase flow is the same order of magnitude as the bubble size in bubbly flow and the film thickness in annular/annular–dispersed flows.

The purpose of the present study is therefore to gain a detailed understanding of the heat transfer mechanisms of liquid metal–gas two-phase flows, in collaboration with flow measurements, in a magnetic field, and thus to provide experimental bases with which theories can be compared. Annular/annular–dispersed flow has been specifically emphasized because of its potential applicability to high efficiency heat removal devices.

2. EXPERIMENTAL APPARATUS AND INSTRUMENTATIONS

A schematic of the liquid metal–gas two-phase flow experimental rig is shown in figure 2. Measurements were conducted at nearly atmospheric pressure for eutectic NaK-78–nitrogen vertically upward flow in a 15.75 mm i.d. and 1.65 mm thick stainless-steel round tube. In order to avoid thermal non-equilibrium between the liquid and gas, the nitrogen gas was heated to the inlet temperature of the liquid before entering the test section. A transverse magnetic field was applied over the distance $z = 460$ to 1460 mm downstream of the test section entrance (figure 3) ($z_B = 0$ to 1000 mm, z_B is the downstream distance from the start of the magnetic field region). The directions of the magnetic field and flow entrance are also shown in figure 3. The field strength ranged from 0 to 0.7 T. Details of the mixing chambers used are indicated in figure 4. Special

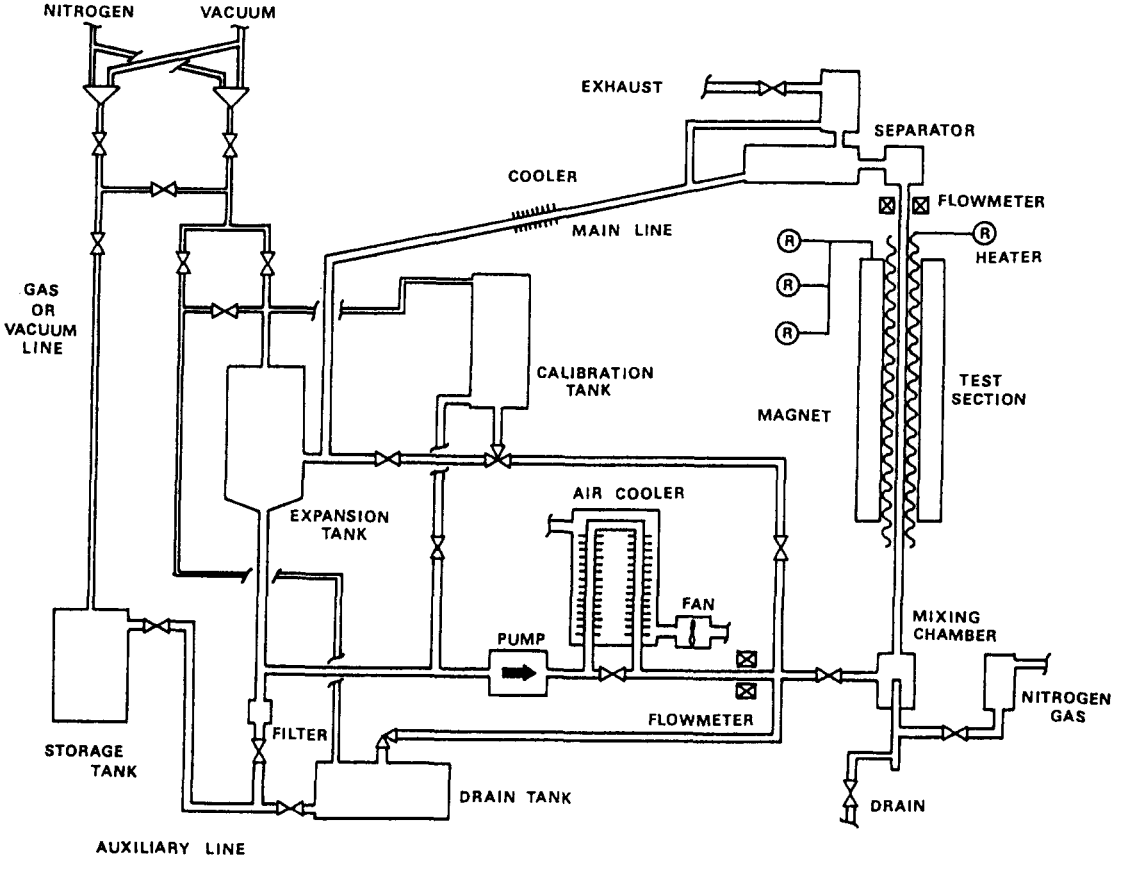

Figure 2. NaK–nitrogen two-phase flow experimental rig.

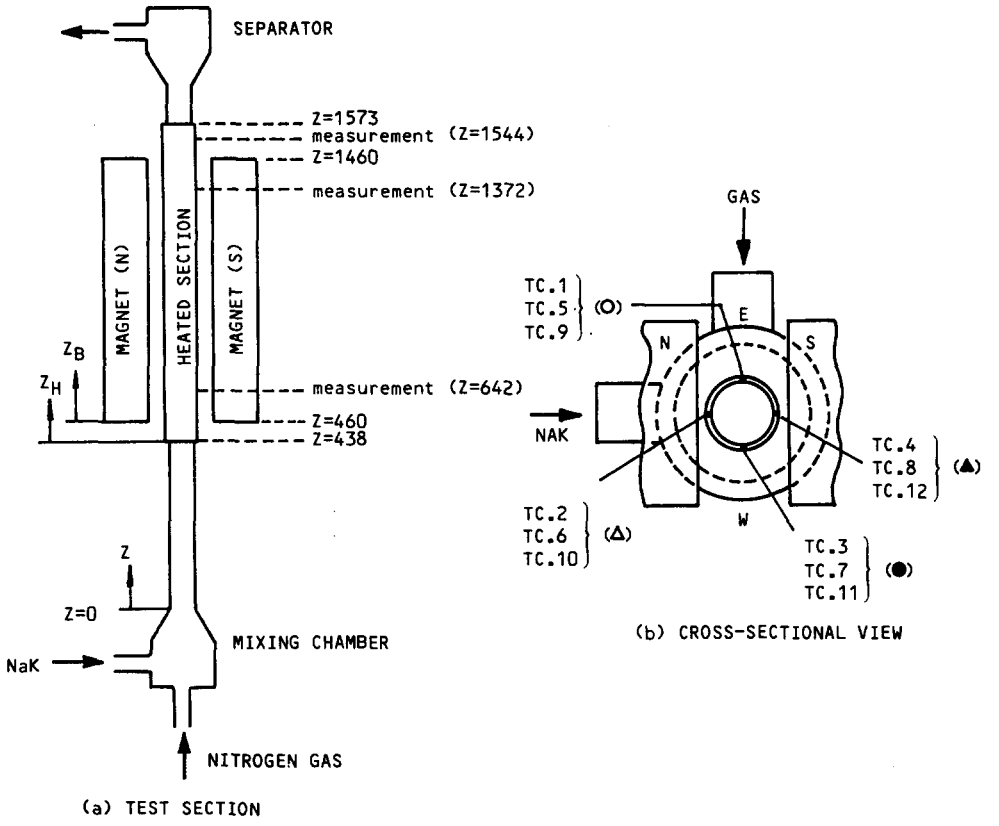

Figure 3. Heat transfer test section and thermocouple locations.

attention was paid to the design of these mixing chambers to avoid any flow instability induced by the gas injection. When the mixer was changed, a slight impact on the flow pattern was observed in bubbly flow, but none in other flow patterns.

Two stainless-steel test sections were prepared in this study, one for flow measurements and the other for heat transfer measurements. These test sections have the same dimensions except for their different measurement accessories (15.75 mm i.d. × 1.65 mm thickness × 1700 mm in length).

The heat transfer test section was uniformly heated by joule heating of doubly-folded 20 μm thick nickel–chrome films with 200 μm thick insulating sheets between the heated strips and between the test section and the inner heated strip. Heat transfer measurements were carried out at constant heat flux of 3.6×10^4 W/m^2.

Thermocouples were embedded at a depth of 0.98 mm from the inner surface at downstream distances from the test section inlet of $z = 642$, 1372 and 1544 mm, as shown in figure 3, along

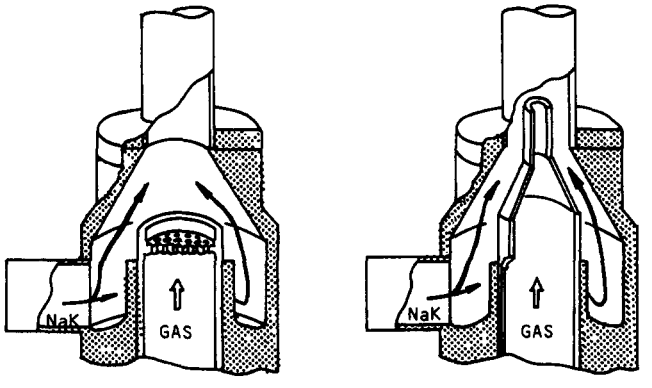

Figure 4. Mixing chambers.

the periphery of the test section at 90° intervals. The thermocouple locations are indicated in figure 3 together with varying symbols which will be used later to represent the measurement results.

Impedance probes of differing designs were used to measure phase distributions, film thickness and surface wave behaviors. Identification of phase change by this method is, of course, based on the electrical conductivity difference between the liquid and gas phases. In our experience with NaK it is very easy to wet almost all materials, forming a liquid bridge (electrical short circuit) between the probe sensors and between the sensor and insulated parts. This liquid bridge greatly reduced the impedance change at phase changes, and the probe signals became saw-tooth in, never on–off binary signals. The signals from one probe sensor were often superimposed on those of another sensor in a pulse-like manner. In addition, the current induced in the mixture flow by the applied magnetic field also affected the probe signals. In order to improve the probe signals by eliminating these effects and to obtain on–off binary signals, we designed and fabricated a hardware system. With this system the probe signals were biased and amplified (gain 1000–1500), and then clipped by the line voltage. The output signal was then fed to a signal processing circuit, similar to that developed by Serizawa *et al.* (1984), in order to get a binary signal representing the change of phase. The probe design should also minimize the above effects.

Several types of electrical resistivity probe were designed and used for different purposes to obtain better results. A typical velocity probe design is shown as an example in figure 5. In all types, the probe tip was 0.2 mm o.d. commercially available polyester-coated copper wire. The temperature range of operation was from room temperature to 70°C. The probe was traversed in the E.–W. directon (perpendicular to the field direction, see figure 3) by linear movement, and also in the N.–S. direction (field direction) by rotating the probe along its axis. In order to make a precise measurement of void fraction and liquid film thickness, the measurement time was 180 s for each point. The estimated error $\Delta\epsilon/\epsilon$ reported here was good to within about $\pm 10\%$.

Two-phase flow patterns were identified based on the probability density function analysis of fluctuating signals from an electromagnetic flowmeter which was located at a position 120 mm downstream of the magnetic field ($z = 1580$ mm) (Michiyoshi *et al.* 1986). For preliminary evaluation of this technique, a double-sensored impedance probe was inserted into the tube center at the axial location $z = 1372$ mm (in the magnetic field) as a back-up system, in order to estimate the flow pattern and also to determine whether or not the flow pattern changed between the two locations. It turned out that no substantial change in the flow pattern took place between the two locations for the range of experimental conditions covered in the present work. During the flow pattern identification experiment, the impedance probe was not placed in the flow in order to avoid flow disturbances induced by the probe.

The wall temperature was estimated from the conduction equation on the basis of the readings of thermocouples embedded in the tube wall. The bulk temperature of the liquid was measured by thermocouples at both ends of the heated section. The average temperature of the mixture at any elevated positions was estimated by linear interpolation, ignoring thermal and MHD entrance effects in the downstream direction. Prior to a series of experiments, this procedure was confirmed to be valid at locations of heat transfer measurement both in single-phase and low-quality two-phase flows with and without a magnetic field by measuring the local mean temperature of the fluid with thermocouples inserted through the heated wall at fixed axial positions. In heat transfer experiments in annular–dispersed flow measurement, we adopted a bundle of four

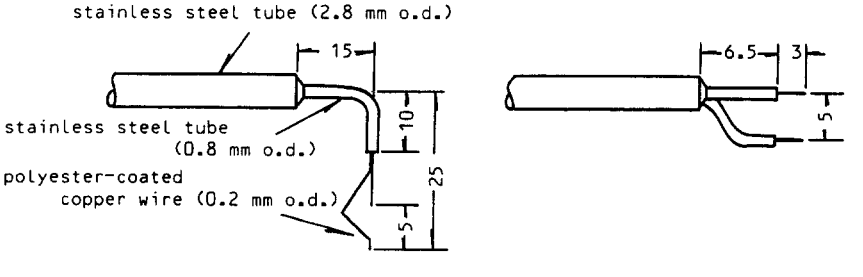

(a) bubble velocity measurement (b) surface wave velocity measurement

Figure 5. A typical design of the impedance probes used for the velocity measurements.

0.5 mm o.d. thermocouples suspended by 0.25 mm o.d. stainless-steel springs to obtain the average liquid film temperature. This bundle of thermocouples was inserted from the upper plenum and separator through the test section down to the end of the heated section. Each thermocouple was kept in slight contact with the inner surface of the test section. In liquid metal–gas annular–dispersed flow the mean film thickness is of the order of 1–2 mm, nearly the same as the thermal boundary layer thickness. Therefore, it was almost impossible to measure accurately the bulk temperature of the liquid film flow. After performing a trial-and-error method, we reached the conclusion that the above-mentioned technique for temperature measurement for film flow gave the best result—since the film temperature measured in this way showed satisfactory agreement with predictions made on the basis of the enthalpy increase calculated from the heat balance at equilibrium conditions (heat loss was estimated to be about 10% of the heat input based on the temperature measurements in an insulating material).

Flow measurements were conducted at temperatures close to room temperature for the inlet condition. Pressures were nearly atmospheric. In the heat transfer experiments the liquid temperature ranged from nearly room temperature to about 35°C at the test section inlet.

3. TWO-PHASE FLOW PATTERNS

Figure 6 shows typical two-phase flow pattern maps for NaK–nitrogen flow with and without a magnetic field. The solid lines in the figure show the experimental flow pattern boundaries and the broken lines show predictions using the Mishima & Ishii (1984) correlation.

As typically shown in figure 6, the Mishima & Ishii correlation predicts well the general trends of NaK–nitrogen flow without a magnetic field. The application of a magnetic field shifted the boundary between bubbly and slug flows, and also that between slug and churn flows, towards lower gas velocity j_G. These changes resulted from the coalescence of small bubbles and the break-up and deformation of long gas slugs induced by the magnetic field, respectively. In general, the application of a magnetic field causes a high pressure gradient which may tend to stabilize the flow and, hence, to promote agglomeration of small bubbles. The transition from bubbly to slug flow thus occurs at smaller j_G. This was verified by a time-sequential trace of the impedance probe signal (figure 7) and also by measuring the bubble chord length and frequency distributions (figure 8). However, when the magnetic flux is very high (not the present case), the flow stabilization induced by the magnetic field might act in a quite different way to maintain bubbly flow to higher velocity levels and void fractions (Petrick *et al.* 1977).

In slug flow with a small void fraction, small bubbles involved in the liquid slugs and also those sticking to gas slugs which crawl near the solid wall tend to coalesce to form larger bubbles or gas slugs due to the same mechanism. On the other hand, in slug flow with a higher void fraction, large gas slugs of a few cm to several tens of cm long (and even larger, e.g. slugs more than 100 cm long were observed in the present experiment) are often encountered. The thin liquid film formed between the solid wall and a large gas slug becomes unstable when the magnetic force exceeds the surface tension force. This results in the break-up of long gas slugs accompanied by the formation of irregular gas–liquid interfaces. This is clearly seen figures 7 and 9. The flow pattern thus changes from slug flow to churn flow.

In annular/annular–dispersed flow, the liquid phase flows in a liquid film on the wall. The occurrence of entrainment and deposition of liquid droplets from and onto the liquid film and also the passage of large disturbance waves cause multidirectional turbulence in the liquid film. By applying a transverse magetic field, the velocity fluctuation in the liquid film might grow in the plane perpendicular to the magnetic field by the inverse energy cascade mechanism (Branover *et al.* 1986; Branover 1986b). In addition, as will be shown later, the amplitude of surface waves on the liquid film also grows with the magnetic field strength, expanding, in some cases, into a high velocity core flow of the gas. The liquid film flow consequently becomes unstable because of the large interfacial drag. When the shear force acting on the film flow at the interface exceeds the surface tension force either entrainment of liquid droplets or disintegration of the liquid film takes place. The magnetic field enhances the generation of droplets and also the break-up of the film in the same way as that mentioned earlier as regarding the slug–churn flow transition. According to the combination of

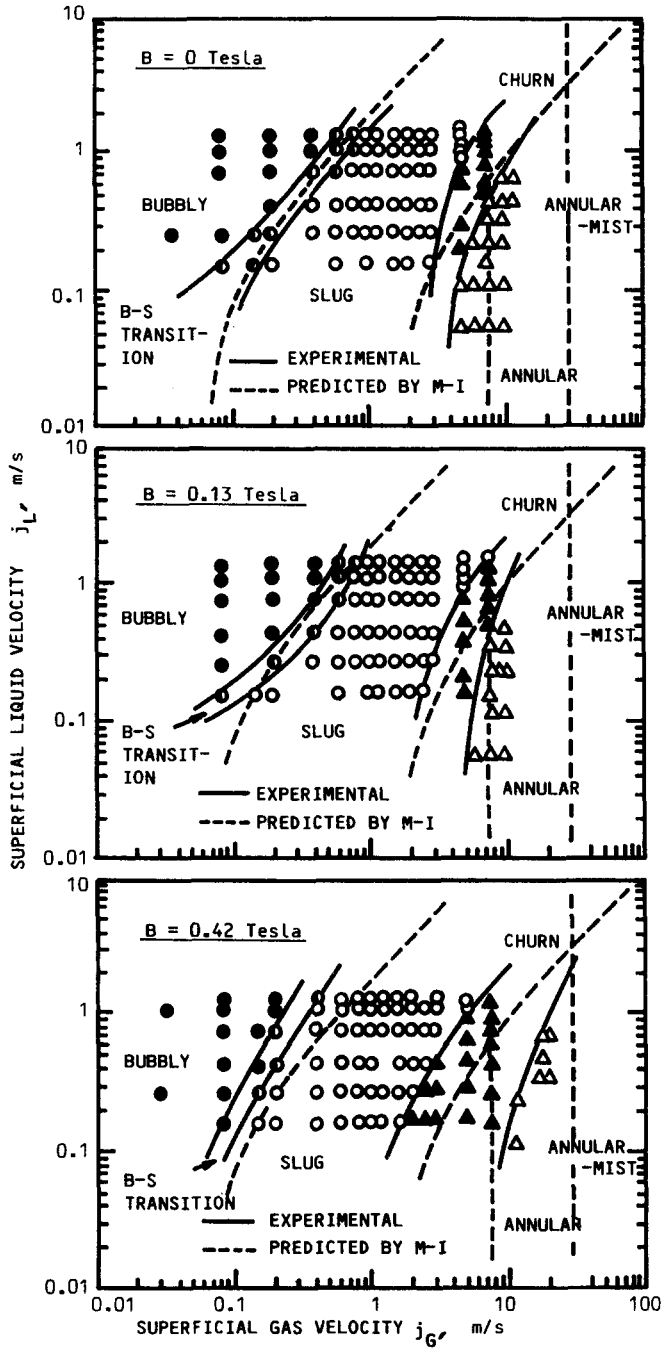

Figure 6. Flow pattern boundaries with and without a magnetic field.

interfacial shear, inertia, surface tension and magnetic forces, the flow changes either to churn flow or to annular–dispersed flow.

Other important magnetic effects are summarized in table 1. It should be mentioned here that all the effects on flow development listed in table 1 are reflected in the heat transfer characteristics, as will be mentioned later.

4. PHASE DISTRIBUTION AND FILM THICKNESS

The magnetic effect on the phase distribution obtained at $z/D = 88$ is demonstrated in figure 10 for low-quality two-phase flows. In the case of no magnetic field, i.e. $B = 0$, radially symmetric

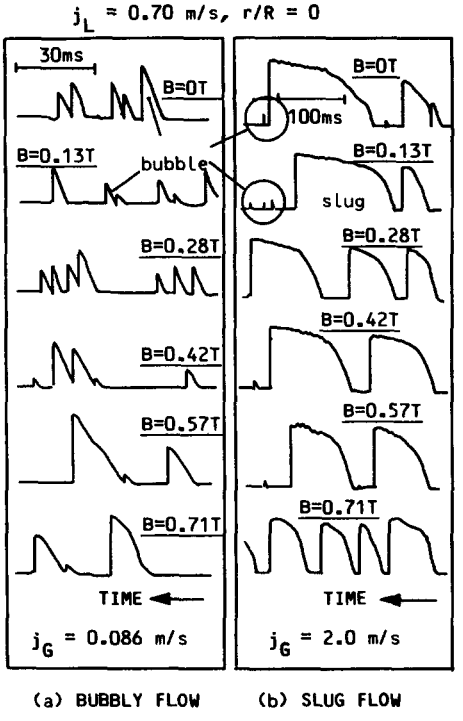

Figure 7. Impedance probe signals.

profiles have been established in bubbly, bubbly–slug transition and slug flows. It is very interesting that the bubbly flow shows a convex profile without wall void peaking. It is well-known that in air–water bubbly flow at liquid velocity $j_L = 0.7$ m/s, the profile is usually concave with wall void peaks (Serizawa & Kataoka 1987). There are possibly two explanations for this. One possibility is the effect of wettability between the solid wall and the liquid, as mentioned earlier. The other is concerned with the bubble size and shape. Based on the chord length distribution measurement (Gakuhari 1986), the mean bubble size in this experiment is estimated to be about 4–5 mm or more, with a wide deviation for spherical bubbles. It is generally accepted that large bubbles tend to collect towards the tube center in vertically upward flow. In air–water flow at atmospheric pressure, a rough criterion for this is about 5 mm. By considering that the fluid-dynamic physical properties

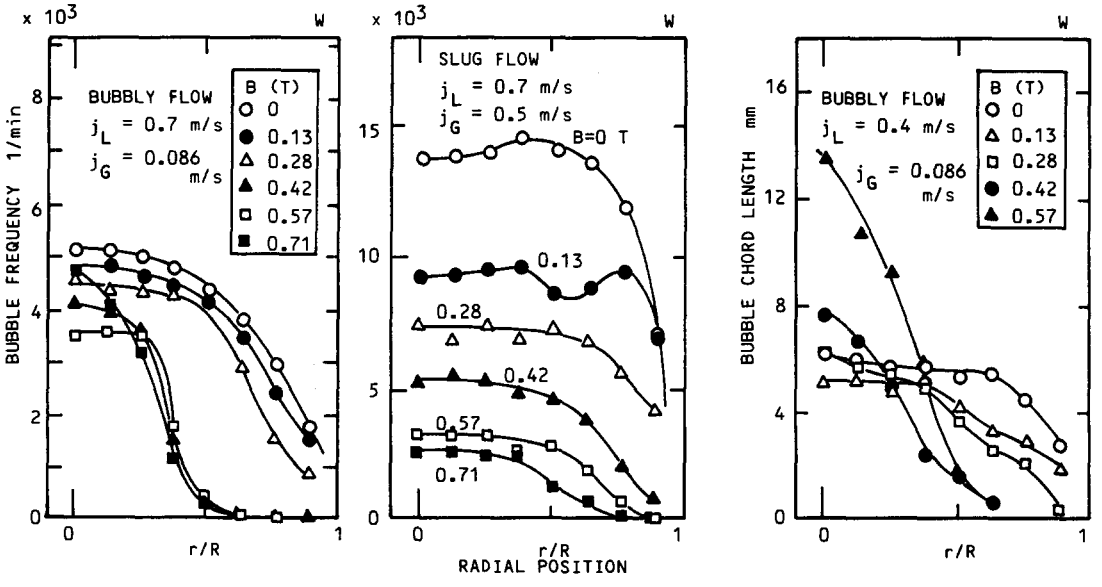

Figure 8. Bubble chord length and frequency distribution.

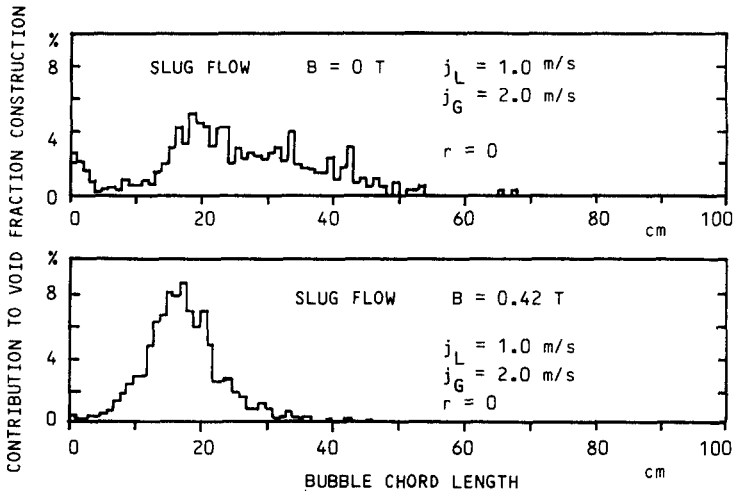

Figure 9. Break-up of gas slugs due to the magnetic effect.

of NaK are rather similar to those of water, this criterion might be roughly the case with NaK also. Therefore, bubbles in this size range observed in NaK–nitrogen flow tend to show a convex void profile.

When the magnetic field was applied, asymmetric profiles were brought about in bubbly flows in the direction perpendicular to the field, E.–W. direction [in figure 10, EW means the traversing direction from the eastern (E) side to the western (W) side, and NS that from the northern (N) side to the southern (S) side, correspondingly with figure 3]. This trend was more typically observed for a stronger field. It should also be noted that these asymmetric profiles did not depend on the direction of the magnetic field [cf. results with $B = 0.42$ and -0.42 T (the negative value means the reverse direction)]. Similar results are reported to have been observed by Michiyoshi *et al.*

Table 1. Summary of the MHD effect on two-phase flow structures

Flow situation		Observed trends ($B < 0.7$ T)	Flow transition
$B = 0$	$B \neq 0$		
BUBBLY FLOW		To enhance bubble coalescence Elongated bubble appear near the wall To decrease the bubble rise velocity An asymmetric phase distribution appears in E.–W. direction To increase the thickness of the near-wall liquid-rich layer	Bubbly → Slug → Smaller j_G
SLUG FLOW		To enhance the coalescence of small bubbles trailed by gas slugs Break-up and deformation of long gas slugs Reduction of the rising velocity of bubbles or slugs To suppress the reversed flow of liquid during the passage of gas slugs	Slug → Churn → Smaller j_G
CHURN FLOW		To enlarge the churn flow region	
ANNULAR FLOW		To increase the thickness of the annular film flow of liquid An asymmetric distribution of the film thickness appears To increase the maximum amplitude of disturbance waves To accelerate the velocity of disturbance waves	Churn → Annular → Larger j_G

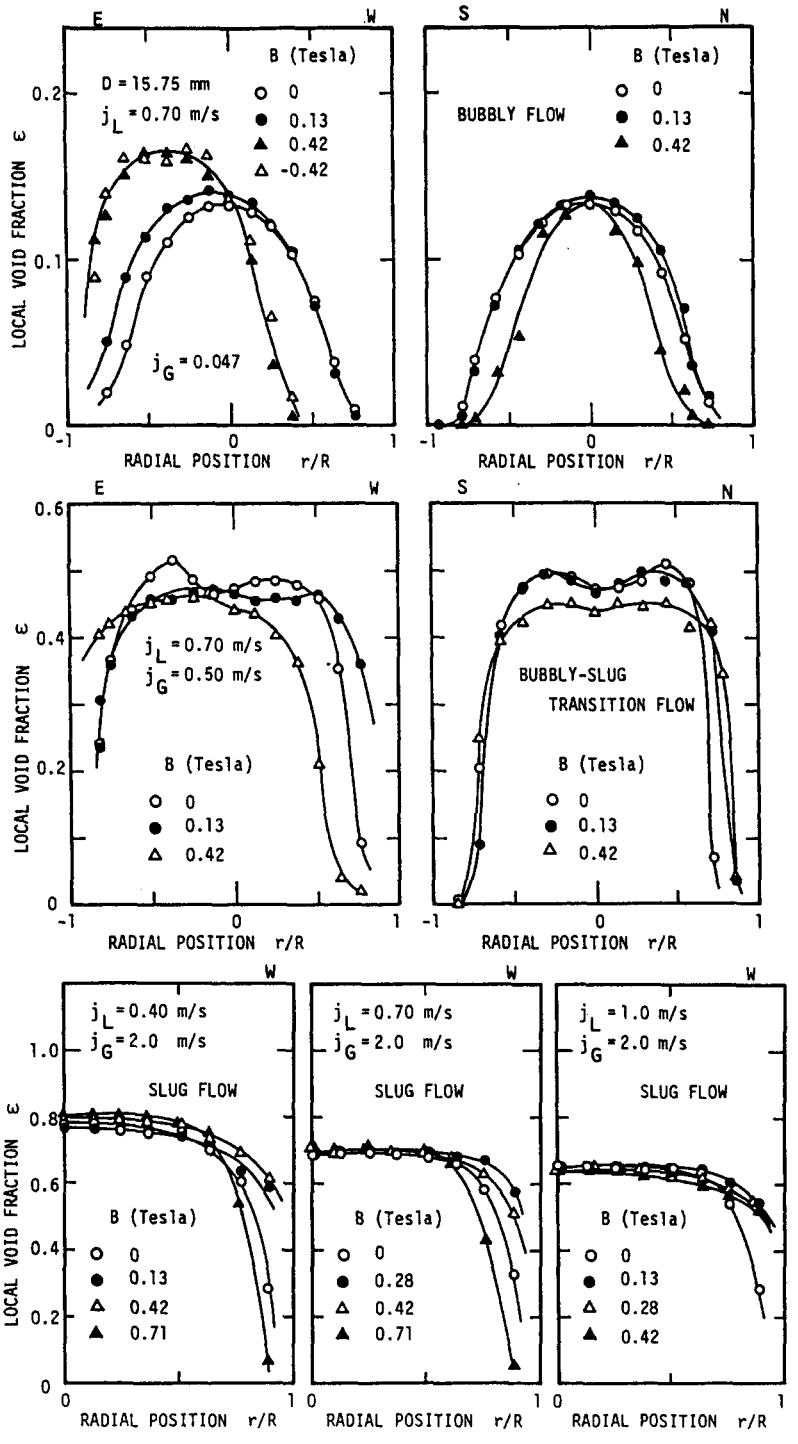

Figure 10. Phase distributions.

(1977) and Gherson & Lykoudis (1984) in mercury–gas two-phase flows. Their interpretation of this phenomenon is that because of the suppression of liquid phase turbulence motions and bubble dispersions caused by the magnetic field, the profile shows the flow distribution established at the beginning of the magnetic field.

In a more recent paper, Lykoudis (1985) presented a comprehensive set of data on the MHD effects on the phase distribution mechanism in vertical and non-vertical mercury–nitrogen down flows. Using a conductivity probe and a video camera, Lykoudis measured and analyzed various types of phase distribution with different methods of bubble injection for various entrance

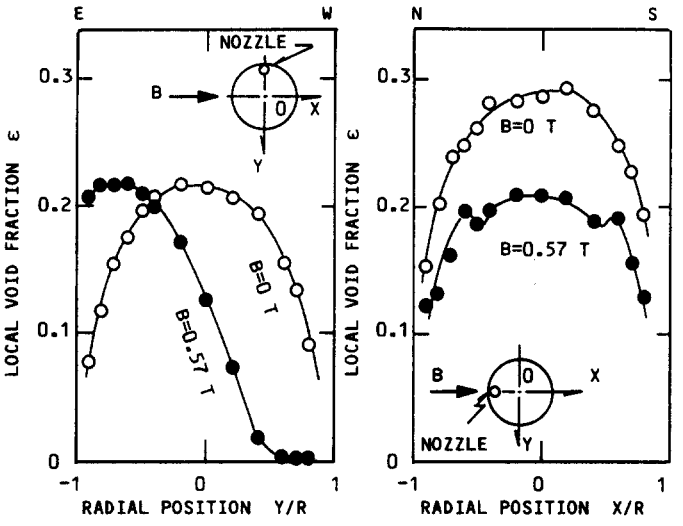

Figure 11. Effect of a magnetic field on the development of phase distributions in mercury–argon flow (Michiyoshi *et al.* 1977).

geometries. He observed that a bubble slightly off the center of the pipe can easily glide in the east or west direction to the east or west corners, where not only is the magnetic pressure zero but the $\mathbf{J} \times \mathbf{B}$ force is also near zero for insulated wall. His conclusion is as follows. The magnetic field dampens both the dispersion and the wobbliness of the bubbles inasmuch as it also dampens the turbulence level of the liquid phase due to both the shear- and buoyancy-induced turbulence. Because of this action, the entrance effects, which are present to some extent, are felt far downstream. He further suggested that when bubbles were injected uniformly from evenly distributed locations in the test section, the competition with the pondermotive ($\mathbf{J} \times \mathbf{B}$) forces and the forces due to bubble interaction with the wall seemed to prevent the bubble concentration from peaking at the center. If, however, large void fractions are created with bubbles originating from vigorous injections at the pipe center only, axisymmetric void distributions are obtained, since the bubbles reaching the wall cannot interact as vigorously as those originating from injection points near the wall.

In their experiments, Michiyoshi *et al.* (1977) measured void fraction profiles with a single nozzle injector located near the wall (either on the northern or eastern side). Some typical results are given in figure 11. When the bubbles were injected from the eastern wall, the profile in the presence of a magnetic field showed asymmetry at a downstream position of $z/D = 73$, which is obviously consistent with Lykoudis' observation. On the other hand, in the case of bubble injection from the northern wall, a symmetric profile resulted. These might be explained by favorable movements of bubbles to the east or west, as mentioned above, but cannot be explained by the entrance effect due to the dampening of the liquid phase turbulence by the magnetic effect.

Figures 12 and 13 show the results of film thickness measurement in annular/annular–dispersed flow without and with a magnetic field, respectively. Here, δ_B, δ_m and δ_c are the base film thickness, mean film thickness and maximum film thickness, respectively. The dimensionless film thicknesses δ_B^+ and δ_c^+ are defined as below:

$$\delta_B^+ = \delta_B \left(\frac{g}{\nu_L^2}\right)^{\frac{1}{3}} \quad \text{and} \quad \delta_c^+ = \delta_c \left(\frac{g}{\nu_L^2}\right)^{\frac{1}{3}}, \qquad [1]$$

where ν_L and g are liquid dynamic viscosity and gravitational force, respectively. The gas Reynolds number Re_G is defined as $Re_G = u_G D_i / \nu_G$, where u_G, D_i and ν_G are the average velocity of the core gas, interface diameter and gas dynamic viscosity, respectively. The maximum amplitude of the disturbance waves on the film surface is shown in figure 14. The Hartmann number for the liquid phase, defined as $Ha = (D/2)B\sqrt{\sigma_e/\mu_L}$, is indicated in figure 13 just for reference, where B, D, σ_e and μ_L are the tube diameter, magnetic field strength, electrical conductivity and viscosity of the liquid, respectively.

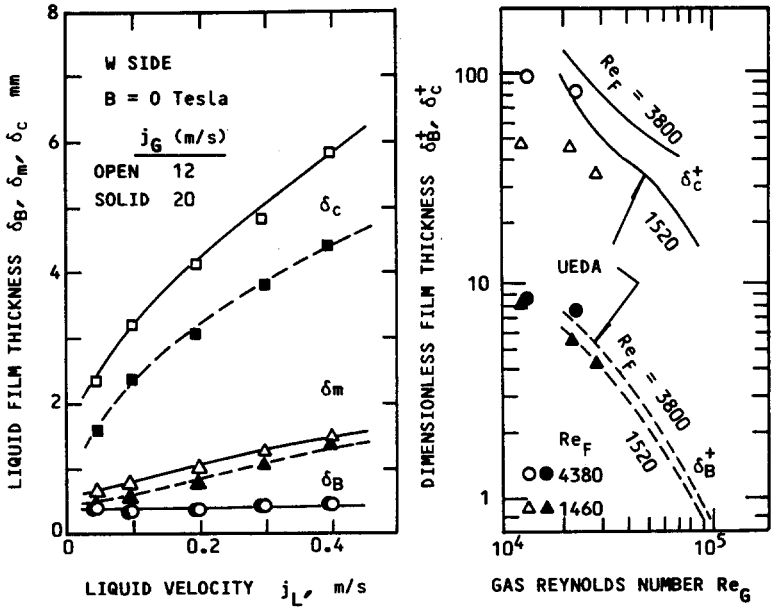

Figure 12. Film thickness measurement without a magnetic field.

As shown in these figures, in the case of no magnetic field, the film flow follows air–water curves (Ueda 1981). When the magnetic field is applied and increased, δ_m and δ_c increase due to the pondermotive forces, whereas δ_B is almost constant. The interesting thing is that the maximum film thickness δ_c and the amplitude $\Delta\delta$ ($=\delta_c - \delta_B$) show maxima at around $B = 0.4$ to 0.6 T, as typically shown in figure 14. This phenomenon is physically interpreted in such a way that large disturbance waves with large amplitudes intruding into the high velocity core flow of the gas, caused by the magnetic effect, can no longer be stable. In some cases, this will be followed by a flow pattern transition from annular to churn flow. In other cases, liquid droplets or liquid lumps may initiate from the crests of disturbance waves. This diversion is thought to depend on the flow conditions. The Ishii & Grolmes (1975) criterion, [2], for the initiation of liquid droplets for a rough turbulent regime calculates a value of about 18 m/s for the critical gas velocity j_{Gc}:

$$j_{Gc}\left(\frac{\mu_L}{\sigma}\right)\left(\frac{\rho_G}{\rho_L}\right)^{\frac{1}{2}} = \left[\frac{\mu_L}{\rho_L \sigma\left(\frac{\sigma}{g\Delta\rho}\right)^{\frac{1}{2}}}\right]^{0.8}. \qquad [2]$$

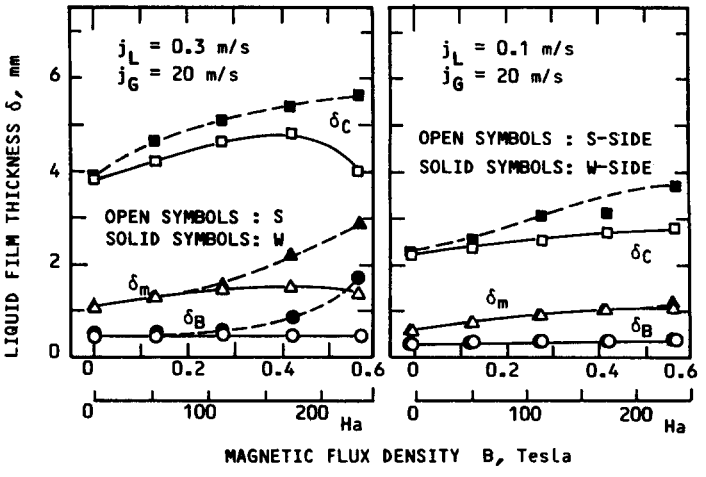

Figure 13. Film thickness measurement with a magnetic field.

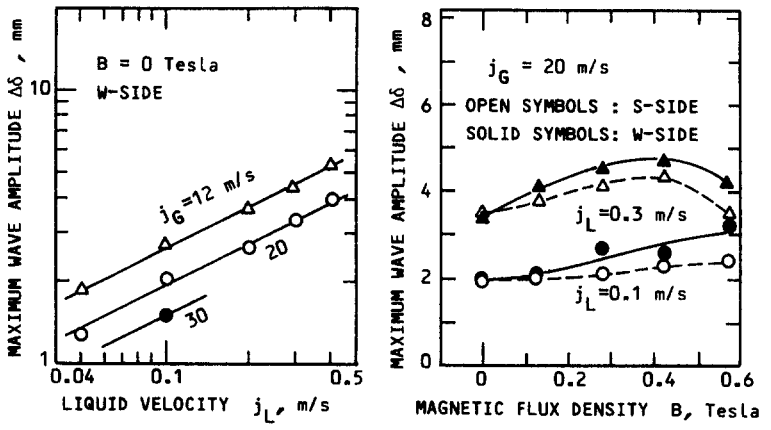

Figure 14. Maximum amplitude of surface waves.

On the other hand, based on the Steen & Wallis (1964) criterion, [3], the critical gas velocity u_{Gc} to initiate significant liquid droplet formation is estimated as 40 m/s:

$$u_{Gc}\left(\frac{\mu_G}{\sigma}\right)\left(\frac{\rho_G}{\rho_L}\right)^{\frac{1}{2}} = 2.46 \times 10^{-4}. \qquad [3]$$

By considering that the mean film thickness was about 2 mm for $j_L = 0.3$ m/s, $j_G = 20$ m/s and $B = 0.4$ T, as shown in figure 13, it is quite reasonable to think that the maxima in the wave amplitude shown in figure 14 are related to the initiation of significant entrainment of liquid droplets. In fact, according to the flow pattern map for $B = 0.42$ T given in figure 6, the flow was consistently annular or annular–dispersed flow, not churn flow.

Tomita *et al.* (1986) investigated experimentally the formation of droplets of a water-based ferrofluid jet falling down through a capillary nozzle in a magnetic field perpendicular to the flow direction. They reported that an increase in the magnetic field enhanced liquid droplet formation due to the Rayleigh instability of the liquid column. They correlated droplet formation with a dimensionless quantity defined as the ratio between the magnetic and surface tension forces. Although interfacial shear was not the controlling mechanism in their experiment, their result was not contradictory to our observation mentioned above.

Another feature found in figures 13 and 14 is the non-symmetric film behavior between the southern and western walls in the presence of a magnetic field. The results indicate a thicker liquid film with a larger wave amplitude on the western wall which is parallel to the magnetic field. This trend was more clearly observed as the field strength was increased. Although this non-symmetric film behavior was not studied further in our experiment, possible mechanisms might be:

(1) The effect of the enhanced anisotropic turbulence induced by the magnetic field, i.e. the formation of a two-dimensional turbulence structure in the film flow.
(2) The effect of interference between the magnetic induced current and the liquid flow (pinch effect).

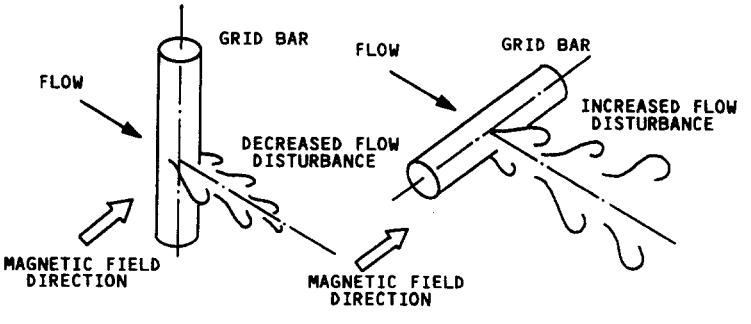

Figure 15. Influence of a magnetic field on grid-generated turbulence.

(3) The effect of a large gradient of magnetic field strength at the inlet and outlet of the magnetic field (end effect).
(4) The Hall effect of charged particles (droplets).

As is well-known in annular/annular–dispersed flow, the liquid and gas phases exchange their momentum and energy through deposition and entrainment of liquid droplets and interfacial drag forces acting at the liquid film–gas interface and at the droplets–gas interface. This process of momentum and energy exchange between the phases causes large-scale turbulence in all directions within the liquid film. In other words, there might be turbulence eddies of similar scale to the flow wake eddies introduced by grids placed in the flow. According to Branover *et al.* (1986; Branover 1986b), when the bars of the perturbing grid are oriented in a direction perpendicular to the direction of the magnetic field, the magnetic field does not enhance the turbulence intensity. On the other hand, when the bars are parallel to the magnetic field and the vortices axes of the flow disturbances have a non-zero projection on the magnetic field direction, the flow disturbances become strongly amplified by the magnetic field (figure 15). Thus, the turbulence is enhanced only in the plane perpendicular to the magnetic field direction, and the three-dimensional turbulence structure is converted into quasi-two-dimensional ones. In such a flow, the turbulence energy is transferred to flow disturbances with low wavenumbers (inverse energy cascade) (Branover *et al.* 1986; Branover 1986b). Therefore, if the liquid film flow has turbulence eddies whose characteristics are similar to those of the grid-generated eddies mentioned above, the turbulence in the liquid film may be enhanced in the direction perpendicular to the magnetic field direction and, hence, the liquid film becomes thicker and surface waves grow more on the eastern and western sides than on the northern and southern sides.

Regarding the second mechanism, the pinch effect can explain qualitatively the experimental trends, but its validity was not quantitatively confirmed by performing an experiment with an additional magnetic field.

The third effect has been analyzed by Oshima *et al.* (1985) for horizontal film flow with a non-conductive wall by solving mass and momentum equations in conjunction with Maxwell's equation and Ohm's law. Their results suggest that the film thickness increases or decreases depending on the field strength, film velocity and film thickness. However, their momentum equation cannot apply to vertical film flows.

Recent numerical calculations revealed, for single-phase liquid flows in a channel, the existence of side layers near the wall in the presence of a transverse magnetic field, i.e. the velocity profiles are M-shaped in the plane perpendicular to the magnetic field (e.g. Branover 1986b). This change in velocity profiles takes place in the zones where the flow enters and leaves the magnetic field. If the channel is conductive, the M-shaped profile persists along the entire flow (Branover 1986a). Although there is no experimental evidence of such velocity profiles reported elsewhere for liquid film flow, such possibilities might exist.

The last mechanism has been recently hypothesized by Lykoudis (1989) in order to explain a certain asymmetric heat transfer behavior between the eastern and western walls in the presence of a magnetic field which will be described later. This hypothesis assumes that the particles (liquid droplets in the present case) will be electrostatically charged during atomization at the test section entrance and show helical movement in the magnetic field. However, unfortunately, we have no direct evidence at the moment to confirm this.

The present authors feel very strongly that it is dangerous to venture to suggest a mechanism (or mechanisms) that explains what has been observed in the present work, since our present knowledge is too limited to draw definite conclusions about the results and, in fact, the research has just begun. However, at the same time, we feel that, in order to gain better insight into heat transfer behaviors which will be stated later, it is necessary to try to present some explanations or interpretations of the mechanisms in spite of the lack of experimental evidence.

5. HEAT TRANSFER EXPERIMENTS

Heat transfer characteristics in low-quality regions were reported in part by Michiyoshi *et al.* (1986). Since then we have continued to carry out measurements with a highly modified test section

and developed more reliable measurement techniques. The present measurements cover the range of flow patterns from bubbly to annular/annular–dispersed flows. However, in this paper we will be mainly concerned with annular/annular–dispersed flow. Only brief descriptions will be given regarding low-quality two-phase heat transfer and the reader is referred to Michiyoshi *et al.* (1986) for further details.

Throughout this study, the heat transfer coefficient h is defined based on the difference between the surface temperature and the interpolated bulk temperature of the mixture or mean temperature of the liquid film on the wall. This temperature difference ranged from about 1 to 25 K under the experimental conditions covered in the present work. Heat transfer results described in the following sections refer to $z = 1372$ mm ($z/D = 87$, $z_H/D = 59$, $z_B/D = 58$; where z_H is the distance in the downstream direction from the beginning of the heated section) unless otherwise stated. In subsequent graphs, the Nusselt number ratio between the magnetic heat transfer and non-magnetic heat transfer, $(Nu)/(Nu)_{B=0}$, is based on the measured Nusselt number for $B = 0$, $(Nu)_{B=0}$.

5.1. Single-phase Heat Transfer

Single-phase heat transfer data are well-correlated in a Pe–Nu diagram over the range Pe = 50 to 600, where Pe and Nu are the Péclet number ($= Re \cdot Pr$, where $Re = j_L D/\nu_L$ and Pr is the Prandtl number of NaK) and Nusselt number ($= hD/\lambda$, where λ is the thermal conductivity of NaK), respectively. Figure 16 demonstrates the measured Nu vs Pe data for no magnetic field. This plot shows that the experimental Nu are about 20–30% lower than the predictions by Subbotin's correlation:

$$Nu = 5.0 + 0.025\,Pe^{0.8}. \qquad [4]$$

The considerable discrepancy observed between the experiments and the predictions mentioned above may be attributed to the effect of dissolved gas or oxides in NaK. It is well-known that liquid metal heat transfer is greatly deteriorated by the thermal conductance which exists between the heated wall and the working fluid, which is due to the high concentration of oxides in a region near the wall (e.g. Kalish & Dwyer 1967). The thickness of this conductance layer is considered to be proportional to that of the laminar sublayer and, hence, inversely proportional to the Re. Therefore, the thermal conductance decreases asymtotically to a certain value with the Re. The present Nu vs Pe data show a trend quite similar to this.

The MHD effect on single-phase heat transfer is demonstrated in figure 17 in an $Nu/Nu_{B=0} - B$ diagram, where Nu and $Nu_{B=0}$ are the Nusselt number with a magnetic field ($B \neq 0$) and that without a magnetic field ($B = 0$), respectively. As a whole, the $Nu/Nu_{B=0}$ ratio indicated a decreasing trend with increasing Pe. This general trend did not alter much as the magnetic field strength B was increased, though the data differed considerably for different thermocouple locations. This deviation of heat transfer for different thermocouple locations is thought to be related to the non-uniform flow distribution induced by the MHD effect.

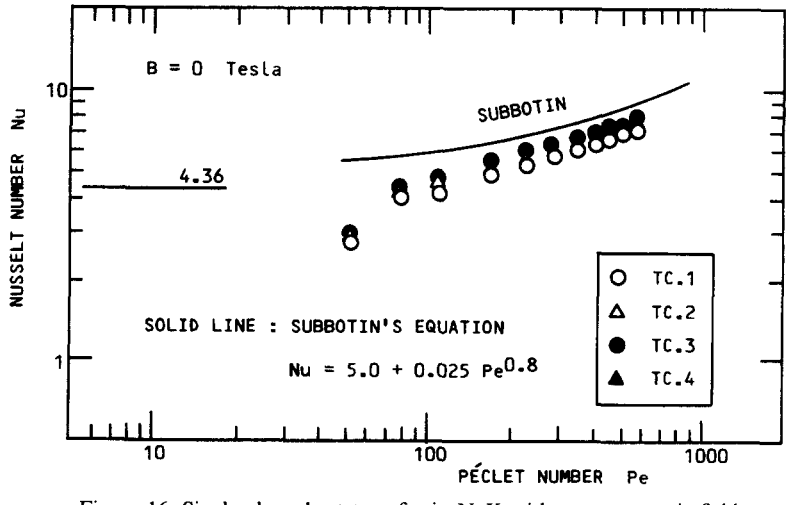

Figure 16. Single-phase heat transfer in NaK without a magnetic field.

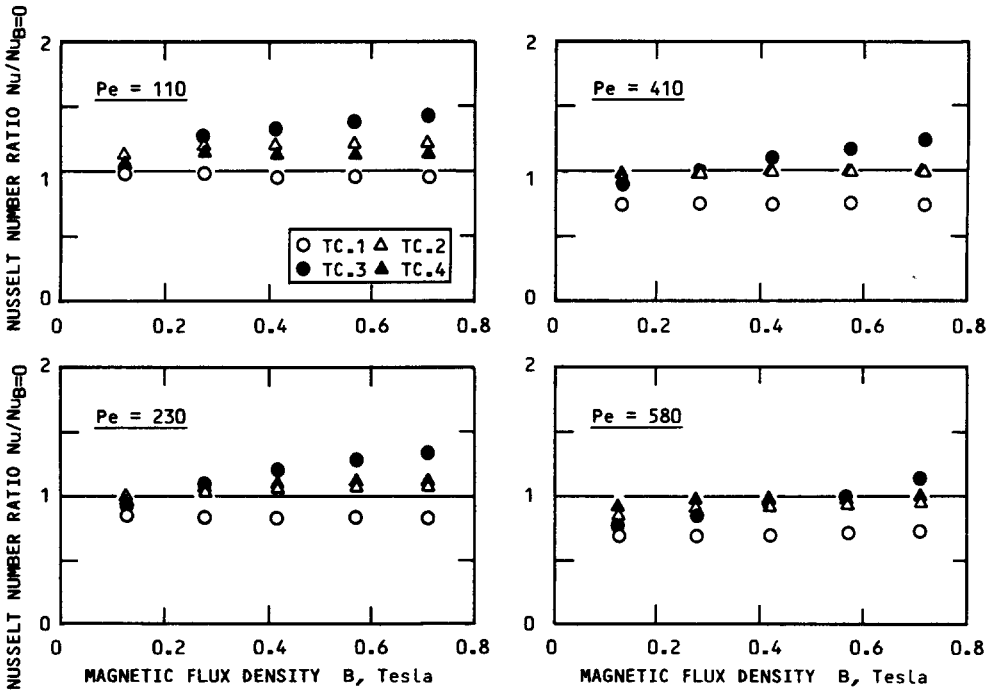

Figure 17. Effect of a magnetic field on single-phase heat transfer in NaK.

Gardner (1968) pointed out for the first time, based on his analysis of laminar flow through an electrically insulated circular tube, that the presence of a transverse magnetic field causes asymmetries that can cause heat transfer enhancement. Regarding the angular dependence of the effect of a magnetic field on Nu, he concluded that, as Ha increases, the local Nu increases more rapidly at the northern (N) and southern (S) walls than at the eastern (E) and western (W) walls, since it reflects the amount of flattening the local velocity profile suffers in the magnetic field. [The velocity profile in the direction parallel to the magnetic field is decelerated in the core and accelerated in the wall region, causing the flat profile. On the other hand, in the direction perpendicular to the magnetic field the flow is decelerated only, but more strongly in the core than near the wall which results in a slight flattening effect (Gardner 1967)]. The present results do not necessarily agree with Gardner's analysis.

Figure 18 presents the maps of turbulent suppression by a transverse magnetic field obtained over the pipe cross section (Lykoudis 1976). In these maps, four regions of relative turbulence intensity are characterized as zones of strong turbulence, moderate turbulence, weak turbulence and laminar flow. As can be seen in figure 18, the turbulence is suppressed very easily along the direction parallel to the magnetic field direction, but not very effectively along the direction perpendicular to the field.

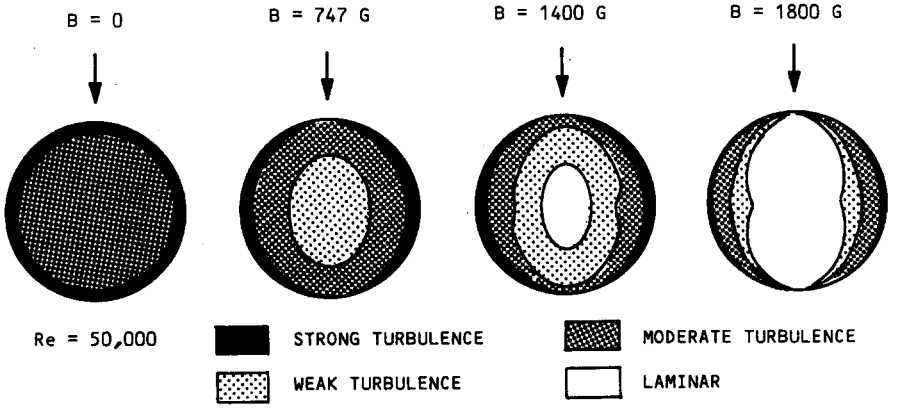

Figure 18. Map of turbulence suppression due to a transverse magnetic field (Lykoudis 1976).

By considering these facts, the local heat transfer behavior with a magnetic field depends on the entire flow field and also on the concentration of oxides or impurities. However, further details have not been clarified in this work.

5.2. Flow Pattern Dependence

As repeatedly described in this paper, two-phase heat transfer is closely linked with two-phase flow patterns. Therefore, it is necessary to have some knowledge of the flow pattern dependence in order to understand the mechanisms involved. Typical results are demonstrated for $j_L = 0.4$ m/s in figure 19, which presents the ratio Nu_{TP}/Nu_{SP} vs the gas volumetric flux j_G, where Nu_{SP} and Nu_{TP} are the single- and two-phase Nusselt numbers for fixed values of the magnetic field strength, respectively. Flow pattern boundaries are also indicated in the figure. Results obtained at other liquid velocity conditions showed trends very similar to those seen in figure 19. The experimental trends observed in the present work for the low-quality region are quite consistent with those previously reported by the present authors (Michiyoshi *et al.* 1986; Michiyoshi 1988).

In the absence of a magnetic field, the bubbly flow heat transfer is determined, as stated earlier, mainly by a balance between the decrease in the effective thermal conductivity of the mixture and the increase in turbulence due to bubble agitation. By referring to the convex phase distribution in bubbly flow given in figure 10, it is understood that there exists near the heated wall a liquid-rich

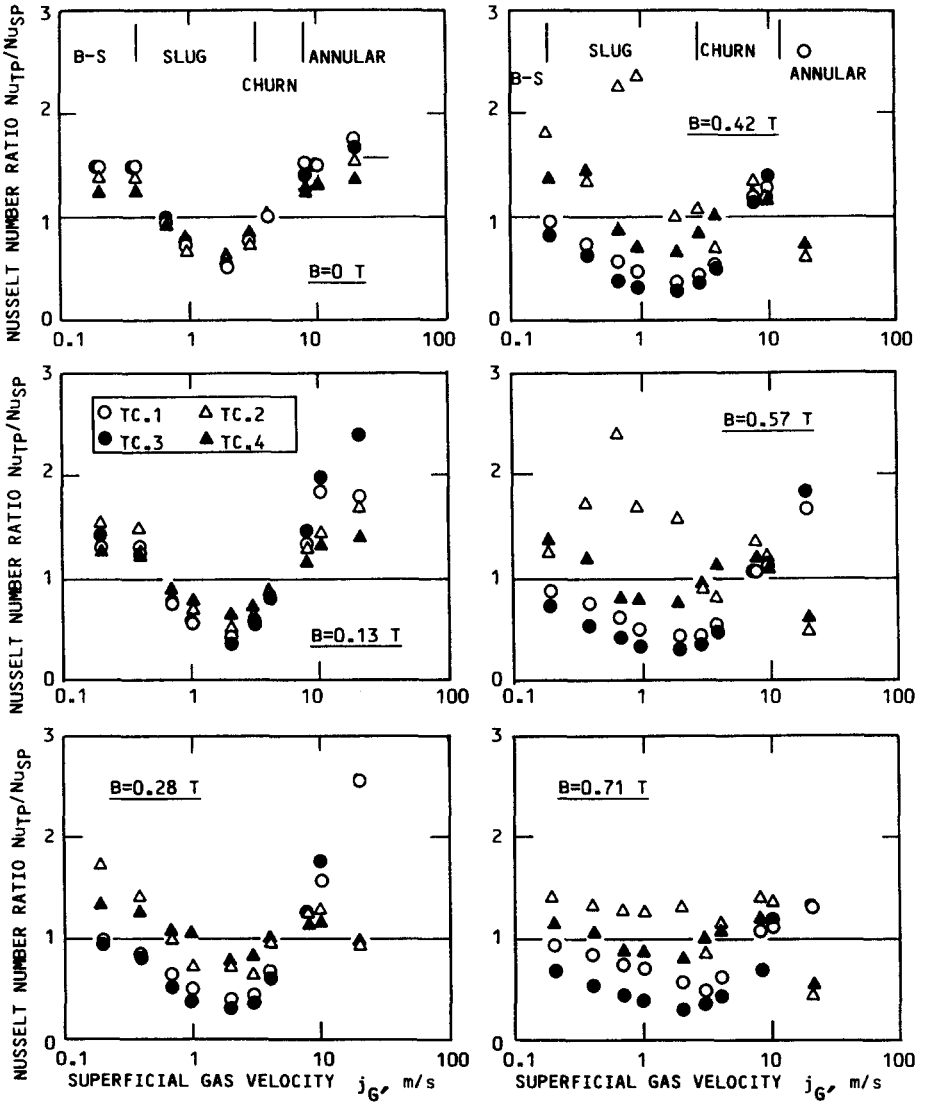

Figure 19. Flow-pattern dependence of two-phase heat transfer ($j_L = 0.4$ m/s).

layer of thickness 2–3 mm, which is nearly the same order of magnitude as the thermal boundary layer thickness. This means that the reduction in the effective thermal conductivity is not considerable in the present case. Therefore, the bubbly flow heat transfer becomes, in general, higher than single-phase heat transfer due to the liquid phase turbulence enhanced by core voids.

Upon detailed inspection of the result in bubbly flow in the magnetic field we may notice that as the magnetic field is increased, the Nusselt number ratio increases remarkably at the northern (TC.2) and southern (TC.4) walls, while at the eastern (TC.1) and western (TC.3) walls it clearly decreases. This trend may be explained as follows. As observed and reported by Lykoudis (1985), and mentioned earlier in this paper, bubbles slightly off the center of the tube tend to glide in the east or west direction to the east or west corners, where not only is the magnetic pressure zero but the $\mathbf{J} \times \mathbf{B}$ force is also near zero for an insulated wall. The stainless-steel test section is, of course, electrically conductive, but its electrical conductivity is of the order 1×10^6 mho/m which is approximately one-quarter of the conductivity of NaK. Therefore, the stainless-steel test section may act as an almost non-conductive wall compared with NaK. In view of Lykoudis' observation, in the present case the bubbles also tend to collect towards the east or west corners. This is, in fact, experimentally verified in figure 10. By virtue of this bubble transport in particular directions in the magnetic field, regions near the northern and southern walls have very low concentrations of bubbles. Therefore, in these regions, heat transfer is greatly enhanced, with respect to single-phase flow heat transfer, by the liquid flow which is accelerated and agitated by bubbles in the flow.

When a gas slug passes in slug flow, reverse flows of liquid have often been observed to occur between the heated wall and the gas slug. Under this condition, liquid phase turbulence in the liquid film is not expected to be enhanced. Therefore, the effects of turbulence enhancement and acceleration of the liquid flow cannot contribute to heat transfer augmentation. The heat transfer coefficient thus decreases as the two-phase flow pattern changes from bubbly to slug flow, notwithstanding asymmetric void fraction profiles such as those shown in figure 10.

When a magnetic field is applied in slug flow, the void fraction profile shows a significant variation with the field strength, as typically indicated in figure 10 (bottom). This change in the void fraction profile in the near-wall region is not well-ordered with the increasing magnetic field. This phenomenon might follow both the coalescence of small bubbles with gas slugs just behind them and the break-up of long gas slugs into smaller ones, both of which are affected by the field strength and inlet flow conditions. In other words, when the magnetic field is applied, the non-uniform flow structure existing at the inlet of the magnetic field is maintained for downstream, more or less, and is even suspected to be amplified by the magnetic field through coalescence/disintegration processes or deformation of bubbles/slugs, and also by bubble motions along the liquid streamline paths deformed by the magnetic field. This hypothetical view is supported partly by measurements of the bubble number density distribution and the bubble/slug length distribution (Gakuhari 1986). Bubble behaviors in the near-wall region are thus reflected in the heat transfer performance in slug flow.

It can be seen from figure 19 that the Nusselt number ratio obtained with thermocouple No. 2 (northern wall) shows a significantly different behavior from those obtained with other thermocouples. In particular, at $B = 0.42$ and 0.57 T, the Nusselt number ratio first increases and then decreases with the gas volumetric flux j_G, having a maximun at $j_G = 0.6$ to 1 m/s. The reproducibility of the result was very good. By considering that the flow pattern under such conditions is slug flow, we may explain this particular heat transfer behavior by assuming that the coalescence/disintegration/deformation processes of bubbles and slugs mentioned above is an important mechanism. On the basis of the work reported by Michiyoshi *et al.* (1977) with nitrogen–mercury flow, it may be supposed that, in the magnetic field, a gas slug can be elongated along the E.–W. direction, while it is compressed along the N.–S. direction because of a higher magnetic pressure. Thus the gas slug may be deformed, followed by formation of a thicker liquid film between the wall and the slug near the northern and southern walls. This thicker liquid film flow might contribute to heat transfer enhancement. The considerable difference in the experimental data between the northern and southern walls may be attributable to the entrance effect of the non-uniform flow structure. When the magnetic field increases beyond about 0.5 T, the liquid film around the slug starts to become unstable because of the increasing actions by magnetic forces,

and the liquid film flow tends to recover its uniformity over the entire cross section of the tube due to the break-up of long gas slugs.

Churn flow is a transition flow from slug to annular/annular–dispersed flow. In this flow pattern, large-scale motions of liquid lumps takes place in a chaotic manner in both the axial and lateral directions. The heat transfer characteristics are therefore recovered and become uniform. The MHD effect on heat transfer is thus reduced. This is clearly seen in figure 19.

Annular flow heat transfer is generally enhanced by convective heat transfer of accelerated liquid film flow. This will be discussed in detail in section 5.3.

5.3. Heat Transfer in Annular/Annular–Dispersed Flow

Typical examples showing MHD effects on heat transfer in annular/annular–dispersed flow are given in figures 20, 21 and 22 for liquid velocities $j_L = 0.2$, 0.4 and 0.7 m/s, respectively. A complete set of data is available in Ida (1988). As can be seen from these figures, nitrogen–NaK data both without and with a magnetic field show quite characteristic behaviors, although the data scatter to some extent. We will describe separately non-magnetic heat transfer and magnetic heat transfer.

5.3.1. Heat transfer without a magnetic field

Regarding non-magnetic heat transfer, the present results show no significant dependence of the ratio Nu_{TP}/Nu_{SP} on the gas velocity j_G. It is widely accepted that the liquid film thickness in annular/annular–dispersed flow generally decreases as the gas velocity increases. This is true with both air–water and nitrogen–NaK flows, as has been shown in figure 12. In ordinary fluid–gas two-phase flow systems such as air–water flows, reduction of the film thickness is usually accompanied by heat transfer augmentation due to forced convection enhanced by the large-scale motions of disturbance waves (Hagiwara 1982) and accelerated liquid film flow, and droplet

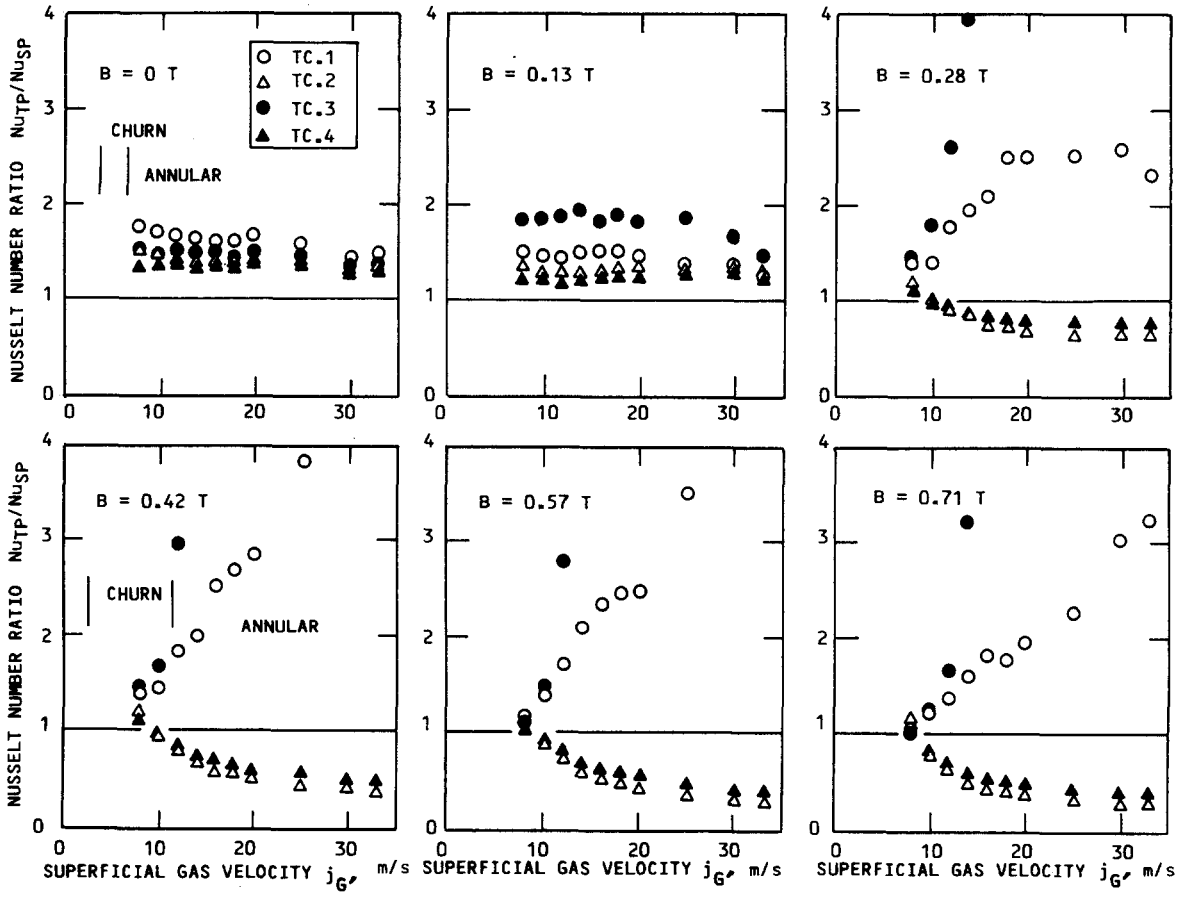

Figure 20. Heat transfer in annular/annular–dispersed flow ($j_L = 0.2$ m/s).

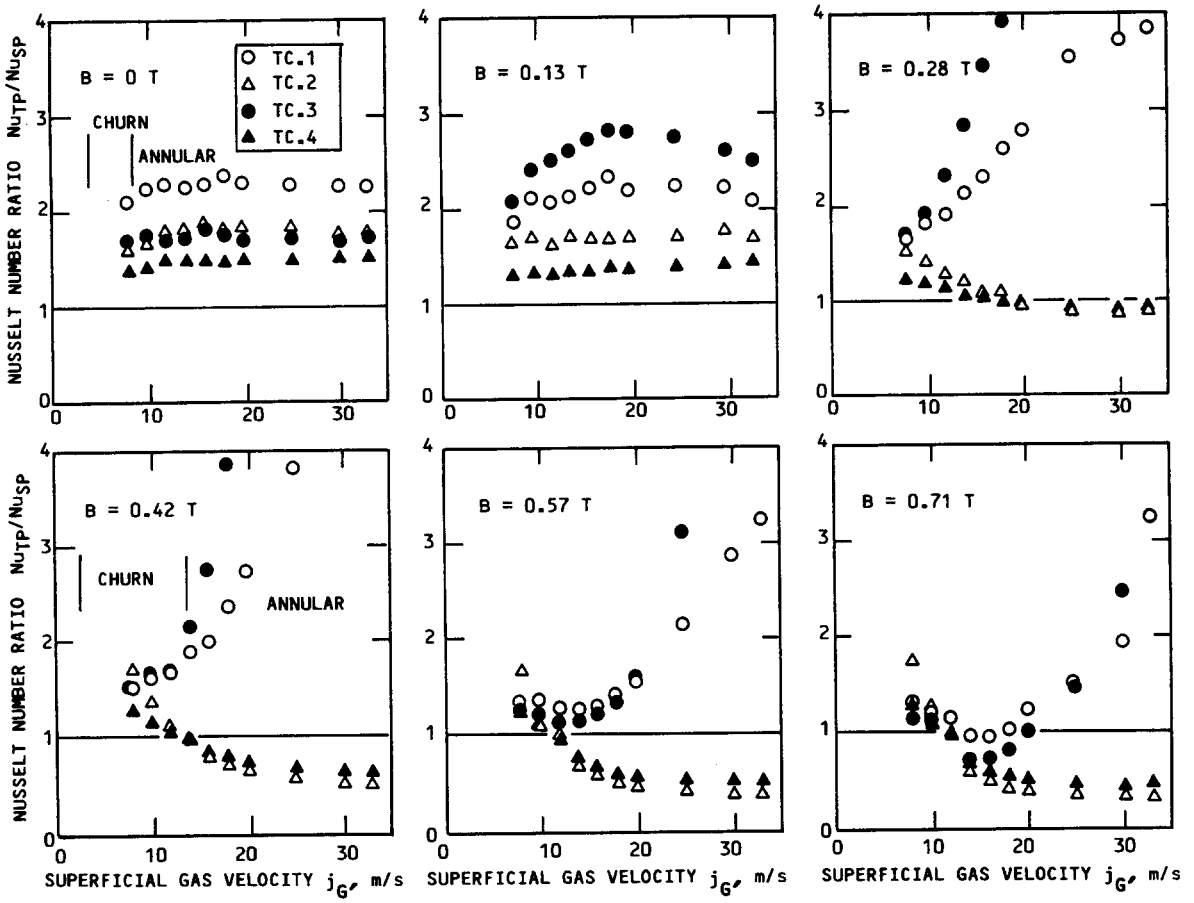

Figure 21. Heat transfer in annular/annular–dispersed flow ($j_L = 0.4$ m/s).

impingement on the heated walls. Air–water annular flow heat transfer is thus generally enhanced by increasing gas velocity. However, the present nitrogen–NaK heat transfer data in the absence of a magnetic field are not affected as much by the gas velocity, and show almost constant Nu_{TP}/Nu_{SP} ratios depending on the liquid velocity j_L.

The reason for this discrepancy between air–water and nitrogen–NaK flows may be explained by the following fact. In air–water flows, the liquid film thickness is of the order of 1–2 mm, which is roughly 10 times the thermal boundary layer thickness (0.1–0.2 mm). Therefore, the conduction contribution is not affected by a decrease in the film thickness. On the other hand, in nitrogen–NaK flows, the thermal boundary layer thickness is of the same order of magnitude as the liquid film thickness (approximately a few mm) due to the high thermal conductivity of the liquid NaK. The conduction–convection contribution through the liquid film therefore reduces significantly as the liquid film thickness decreases. It is thus understood that the nitrogen–NaK annular flow heat transfer is therefore determined by a balance between the reduced conduction–convection contribution resulting from the decrease in the liquid film thickness and the convective contribution enhanced by the accelerated liquid film flow with massive agitation by disturbance waves and by droplet impingement causing thermal boundary layer agitation. As a result of this balance, the heat transfer characteristic does not show a significant j_G dependence—in contrast to air–water flow. In view of the fact that annular/annular–dispersed flow requires a long distance, of the order a few hundred diameters, to attain developed flow conditions, the slight difference in trends between different thermocouple locations is thought to be related to the entrance effects. This explanation is supported by comparing in figure 23 the results obtained at downstream positions $z = 642$ mm ($z/D = 41$, in the magnetic field) $z = 1372$ mm ($z/D = 87$, in the magnetic field) and $z = 1544$ mm ($z/D = 98$, out of the magnetic field). In this figure, the aforementioned difference shows a decreasing trend with increasing downstream distance.

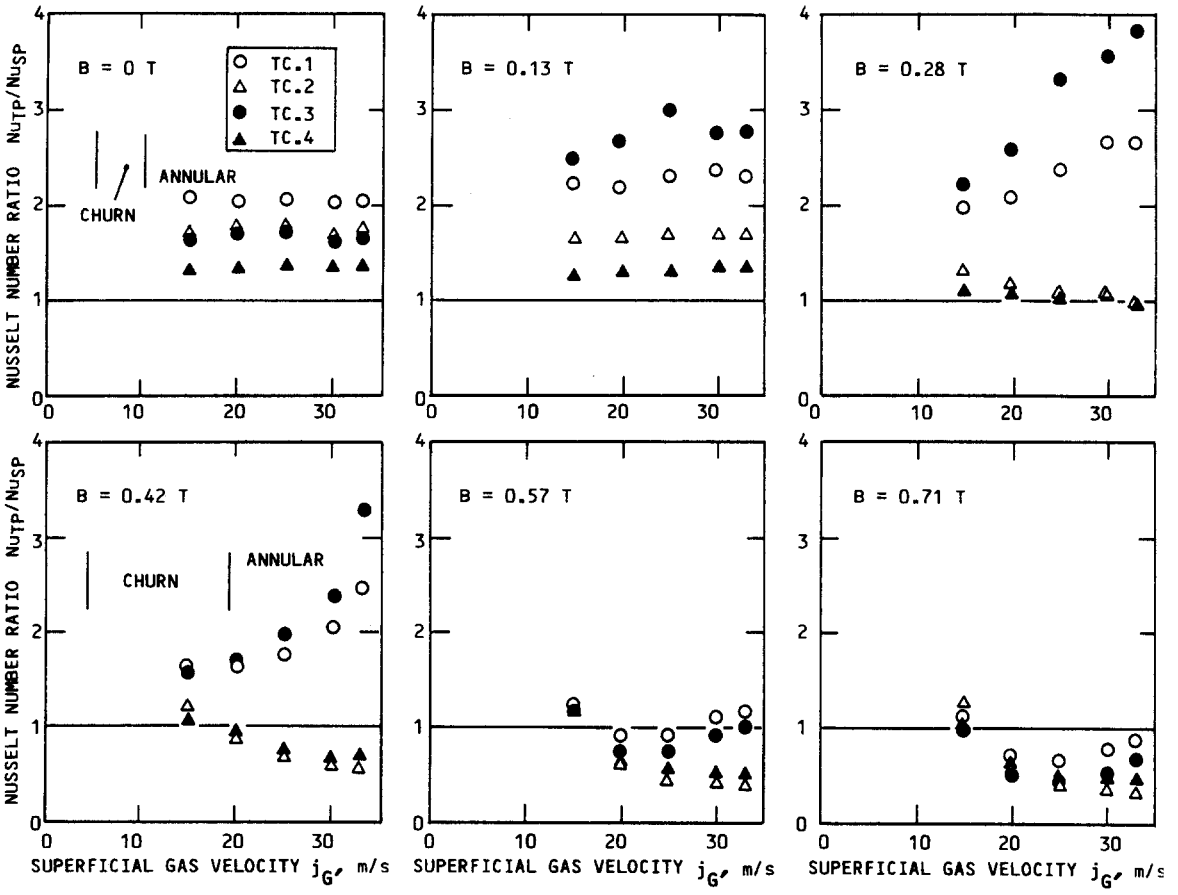

Figure 22. Heat transfer in annular/annular–dispersed flow ($j_L = 0.7$ m/s).

5.3.2 Heat transfer with a magnetic field

Two distinct features of the MHD effect on nitrogen–NaK annular/annular–dispersed flow can be clearly seen in figures 20–22:

(1) Asymmetric heat transfer characteristics between the surfaces parallel to the direction of the magnetic field (eastern and western walls: TC.1, TC.3) and those perpendicular to the field direction (northern and southern walls: TC.2, TC.4).
(2) Asymmetry between the eastern and western walls.

Regarding the first asymmetry, it is generally understood from these figures that application of a magnetic field brought about a significant enhancement of heat transfer on the heated walls parallel to the field direction. So far as this is concerned, the present result is not contrary to the observation of Inoue *et al.* (1987) that heat transfer was enhanced at the bottom surface of a horizontal rectangular channel which was parallel to the field direction (figure 1). However, on the heated walls perpendicular to the magnetic field direction, heat transfer was considerably deteriorated. It should be noted here that the flow limits of j_L and j_G at which this asymmetry appears roughly coincide with the flow pattern transition from churn to annular flow. This variation of heat transfer with thermocouple location observed in annular/annular–dispersed flow was the reverse of that observed in slug flow.

It is, however, noted that this asymmetry depends on the field strength. When the magnetic field is smaller than about 0.4 T, the asymmetry increases with increasing field strength. For field strengths exceeding 0.4 T, the asymmetry is a decreasing trend. By referring to figure 14, which shows a maximum in the wave amplitude at a field strength of $B = 0.4$ T, and by considering that the disturbance waves play an important role in the heat transport process in annular/annular–dispersed flow because of their large-scale convection and agitation effects (Hagiwara

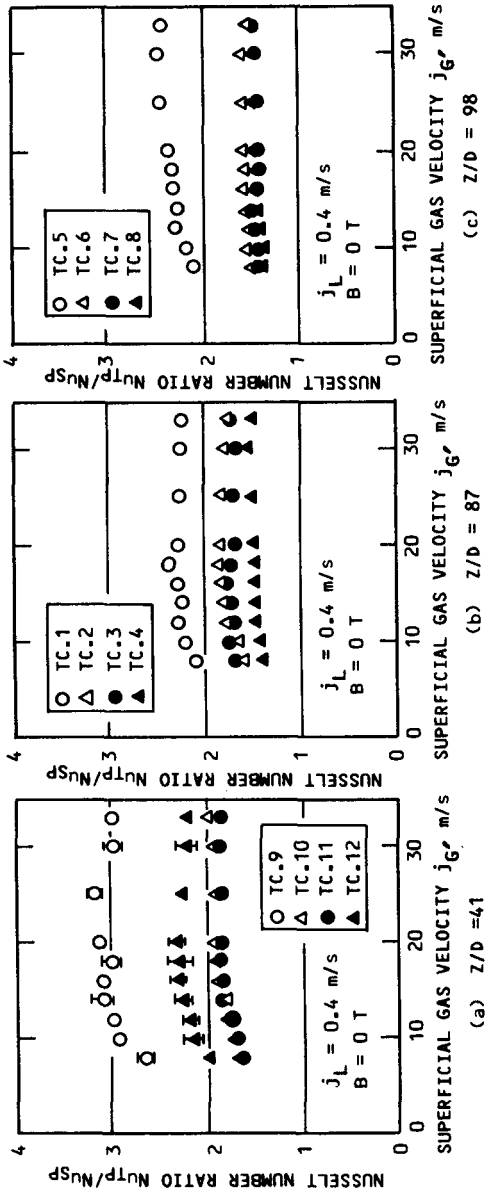

Figure 23. Entrance effect on annular/annular–dispersed flow without a magnetic field.

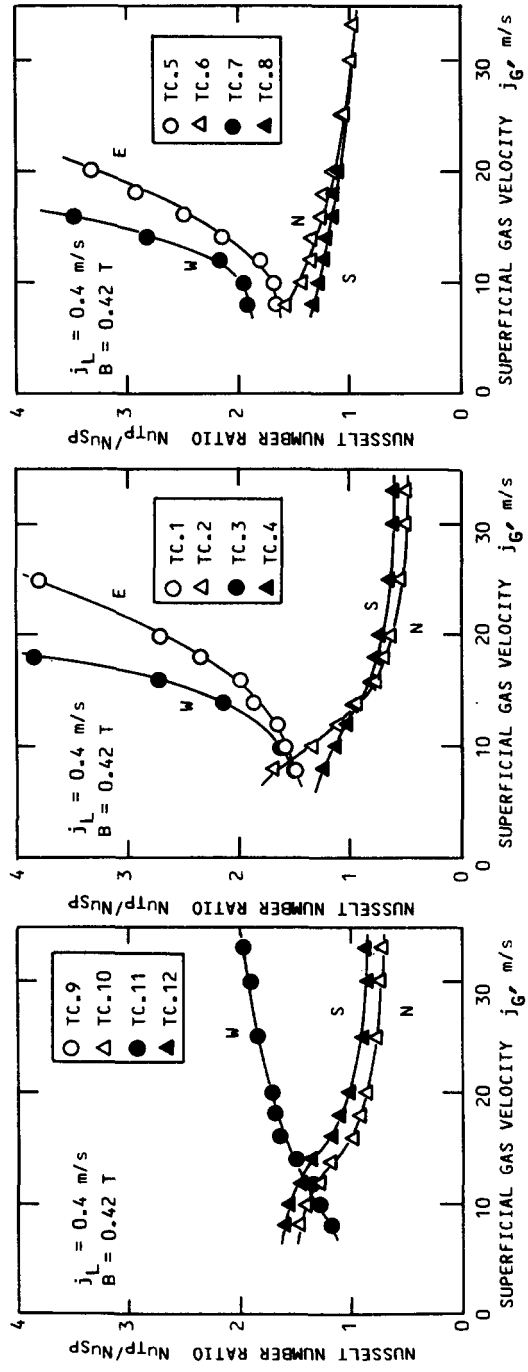

Figure 24. Variation of asymmetric heat transfer between surfaces (E, W) and (N, S) along the flow direction.

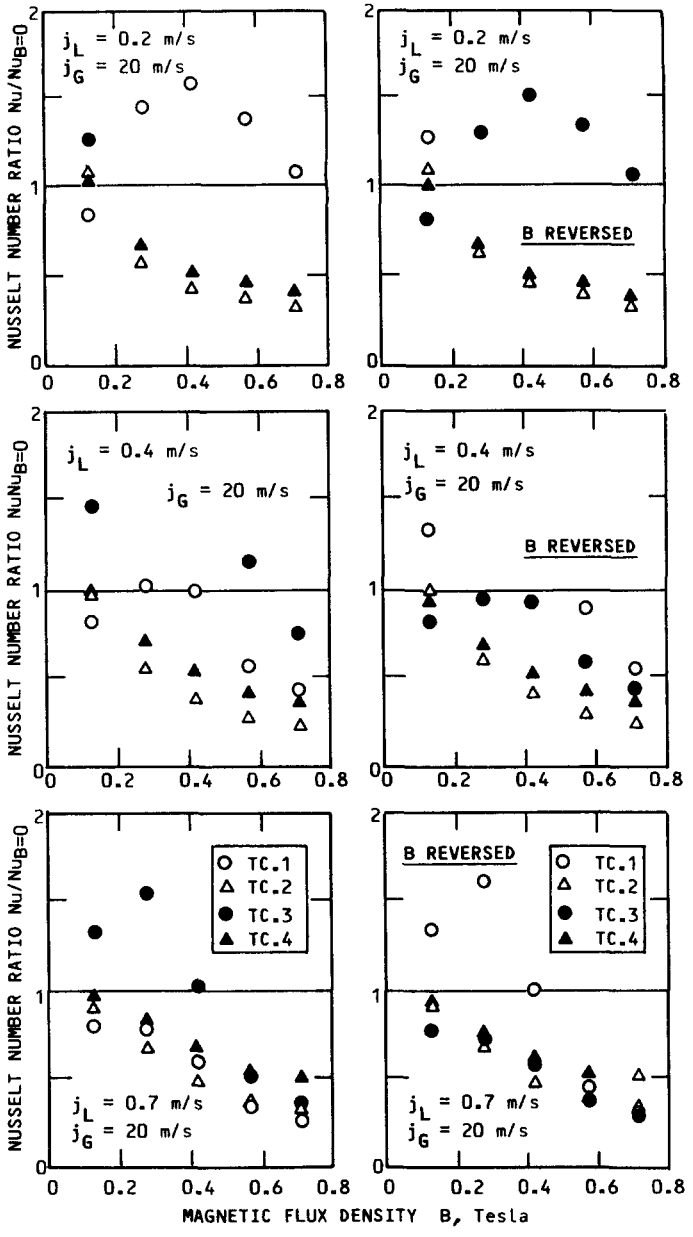

Figure 25. Effect of the magnetic field direction on the second type of asymmetry.

1982), it is apparent that the MHD effect on multidimensional behaviors of disturbance waves (initiation, growth and break-up) is likely to be one of the reasons for the asymmetry mentioned above.

Another explanation is that the asymmetric heat transfer behavior could be related to the liquid phase turbulence in the film flow. On heated surfaces parallel to the magnetic field direction, the azimuthal turbulence component is not affected by the field. On the other hand, on heated surfaces perpendicular to the field, the pondermotive force acts in such a way that the azimuthal flow component is suppressed. This might result in heat transfer deterioration on these surfaces. This is, of course, one of two possible hypotheses relating to the film flow turbulence. The second possibility is as follows. In single-phase pipe flows, as already shown in figure 18 which has been taken from the work of Lykoudis (1975), the turbulence is suppressed along the direction parallel to the magnetic field, while along the direction perpendicular to the field the turbulence is less suppressed. If the magnetic force acts on the film flow in annular/annular–dispersed flow in the same way as in single-phase liquid flow, the liquid phase turbulence in the film may be highly suppressed at the northern and southern walls and less suppressed at the eastern and western walls.

So that the film flow turbulence is, after all, determined by the accelerated liquid film flow superimposed by the magnetic effect which causes the reduction in the turbulence level as mentioned previously. Although we did not perform numerical calculations of velocity profiles within the liquid film in a magnetic field, we believe that the velocity profiles in the film are also affected by the magnetic forces as in single-phase liquid-flow. This might lead to the existence of something like side layers in the film flow which could enhance heat transfer at the eastern and western walls.

Figure 24 shows the development of this asymmetric heat transfer behavior along the flow direction. From this figure, it is concluded that the asymmetry becomes greater with increasing downstream distance in the magnetic field, and less noticeable in the zone outside the magnet. It is thus reasonable to consider that this asymmetric heat transfer behavior is not brought about by a sudden change in the magnetic field at its inlet and outlet. It is, consequently, suggested that the MHD effect on the local flow structure integrated over the entire magnetic region (we call this the "history effect" in this paper) is important in determining the local heat transfer behavior.

Finally, some discussions will be given as to the second asymmetry, i.e. the asymmetry between the eastern and western walls (both are parallel to the field). If this asymmetry is assumed to be the result of an abrupt change in the local flow structure encountered when the flow enters the magnetic field (end effect) or the result of the entrance effect sustained by the magnetic field mentioned previously, the trend of the heat transfer data will not be changed by reversing the magnetic field. We examined this by applying the field in a reverse way. Results were very reproducible and are given in figure 25, showing a complete reversal in the trend. Namely, the new western wall showed higher heat transfer again than the new eastern wall, as before. It thus depends obviously on the direction of the magnetic field. We also observed less remarkable asymmetry of this type at the more upstream location $z = 642$ mm. From these results we conclude that the second type of asymmetric heat transfer behavior between the eastern and western walls is also due to the integrated MHD effect (history effect) again. In order to explain this phenomenon, Lykoudis suggested the Hall effect due to liquid metal particles which could carry electric charge when the droplets are formed through atomization (Lykoudis 1989). This Hall effect could cause a difference in the particle depostion–departure mechanism that takes place on the walls. However, unfortunately, the present authors have found neither direct experimental evidence nor theories to date which can reasonably explain this second asymmetry, particularly the effect of field polarity.

6. CONCLUSIONS

The following conclusions were drawn from the work presented in this paper. However, the authors feel strongly that the hypothetical views presented in this work should be proved or disproved by future studies:

1. Two-phase flow patterns were observed and presented in a map. The MHD effect on flow pattern transitions was also presented and discussed. The outline of this effect is summarized in figure 6 and table 1.
2. Phase distributions in bubbly, bubbly-to-slug transition and slug flows were measured. No wall void peaking was observed in bubbly flows. It has also been found that in bubbly flows the application of a magnetic field brought about a significant asymmetric phase distribution profile in the direction perpendicular to the field. This asymmetric phase distribution in bubbly flow was not dependent on the field direction. While in slug flow, the profiles varied significantly with the field strength in a very complicated manner, especially in the near-wall region. This variation of the near-wall void fraction is thought to be reflected in the local heat transfer behavior.
3. Film thickness and surface waves in annular/annular–dispersed flows were measured without and with a magnetic field. In the case of no magnetic field, the film behaviors followed the general trends reported for air–water flows. When a magnetic field was applied, the film thickness showed an increasing trend with the magnetic field. The maximum amplitude of surface waves showed a maximum at a field strength of nearly 0.4 T. This phenomenon is suspected to be related to the initiation of significant liquid droplet formation.

4. The application of a magnetic field induced a circumferentially non-uniform film flow behavior in annular/annular–dispersed flow. In a magnetic field, the liquid film was thicker on the walls parallel to the field direction. Although some discussions were presented on this, the mechanism was not clarified.
5. The two-phase heat transfer characteristics indicated a clear dependence on two-phase flow patterns, similarly to those in ordinary liquid–gas systems. However, it has been found that the local heat transfer behavior in NaK–nitrogen flow is more closely linked with local two-phase flow structures near heated walls than in ordinary fluid systems. The reason is that, due to the high thermal conductivity of liquid metals, the thickness of the thermal boundary layer formed on the heated surfaces becomes of the same order of magnitude as the bubble size and liquid film thickness in annular/annular–dispersed flow.
6. Annular/annular–dispersed flow heat transfer without a magnetic field indicated almost no dependence on the gas velocity j_G. Increasing the gas velocity decreased the liquid film thickness. This resulted in a reduction of the conduction–convection contribution.
7. In the magentic field the local heat transfer behavior in annular/annular–dispersed flow indicated an angular dependence, due to the circumferentially non-uniform flow structure induced by the MHD effect. Two types of asymmetric heat transfer behavior were observed.
8. The first asymmetry is that observed between the surfaces parallel and perpendicular to the magnetic field. By increasing the field strength, heat transfer was enhanced on surfaces parallel to the field, whereas on surfaces perpendicular to the field heat transfer deteriorated. This type of asymmetry can be explained by circumferentially non-uniform liquid film flow structures.
9. The second asymmetry is that between two surfaces which are both parallel to the field. This asymmetry showed a clear dependence on the magnetic field polarity, but it was not affected by a sudden change in the magnetic field strength. This mechanism has not been made clear in the present work. However, from both academic and practical point of view, this should obviously be clarified in future studies.

Acknowledgements—The authors would like to acknowledge the support of this work by a Grant-in-Aid for Scientific Research from the Ministry of Education, Science and Culture of Japan. They are also grateful to Professor P. S. Lykoudis of Purdue University for his available discussions and suggestions.

REFERENCES

BENDER, J. D. & HOFFMAN, M. A. 1977 A two-phase flow cooling concept for fusion reactor blankets. LLNL Report UCRL-78892.

BRANOVER, H. 1986a Liquid-metal MHD. In *Proc. 9th Int. Conf. on Magnetohydrodynamic Electrical Power Generation*, Tsukuba, Japan, pp. 1735–1749.

BRANOVER, H. 1986b Experimental studies in liquid–metal magnetohydrodynamics. In *Proc. 9th Int. Conf. on Magnetohydrodynamic Electrical Power Generation*, Tsukuba, Japan, pp. 737–748.

BRANOVER, H., MOND, M., PIERSON, E. S. & WALKER, J. S. 1984 Magnetohydrodynamic flows and turbulence: a report on the *4th Beer-Sheva Seminar*. *J. Fluid Mech.* **147,** 461–476.

BRANOVER H., SUKORIANSKY, S., TALMAGE, G. & GREENSPAN, E. 1986 MHD considerations in the design of self-cooled liquid–metal blankets for fusion reactors. In *Proc. 9th Int. Conf. on Magnetohydrodynamic Electrical Power Generation*, Tsukuba, Japan, pp. 764–773.

GAKUHARI, K. 1986 Local properties of liquid metal–gas two-phase flow in a magnetic field (in Japanese). M.S. Thesis, Kyoto Univ. Japan.

GARDNER, 1968 Laminar pipe flow in a transverse magnetic field with heat transfer. *Int. J. Heat Mass Transfer* **11,** 1076–1081.

GHERSON, P. & LYKOUDIS, P. S. 1984 Local measurements in two-phase liquid–metal magneto-fluid-mechanic flow. *J. Fluid Mech.* **147,** 81–104.

HAGIWARA, Y. 1982 A study of flow characteristics and heat transfer of annular and dispersed two-component two-phase flows. Doctoral Thesis, Kyoto Univ. Japan.

IDA, T. 1988 Heat transfer of NaK–nitrogen annular–dispersed flow in a magnetic field (in Japanese). M.S. Thesis, Kyoto Univ. Japan.

IDA, T., SERIZAWA, A., TAKAHASHI, O. & MICHIYOSHI, I. 1988 Heat transfer in two-phase annular flow of NaK–nitrogen under a magnetic field. *Proc. 25th natn. Heat Transfer Symp. Japan* **2,** 103–105.

INOUE, A., ARITOMI, M., TAKAHASHI, M., NARITA, Y., YANO, T. & MATSUZAKI M. 1987 Studies on MHD pressure drop and heat transfer of helium–lithium annular–mist flow in a transverse magetic field. *JSME Int. J.* **30,** 1768–1775.

ISHII, M. & GROLMES, M. A. 1975 Inception criteria for droplet entrainment in two-phase cocurrent film flow. *AIChE Jl* **21,** 308–318.

KALISH, S. & DWYER, O. E. 1967 Heat transfer to NaK flowing through unbaffled rod bundles. *Int. J. Heat Mass Transfer* **10,** 1533–1558.

LIELAUSIS, O. 1975 Liquid–metal magnetohyrodynamics. *Atom. Energy Rev.* **13,** 527–581.

LYKOUDIS, P. S. 1976 Short description of current work in the MFM laboratory of Purdue University. In *MHD—Flows and Turbulence* (Edited by BRANOVER, H.), pp. 103–118. Wiley, New York.

LYKOUDIS, P. S. 1985 Liquid–metal magneto-fluid-mechanic turbulence. In *AIAA Aeronautics and Astronautics Series*, Vol. 100 (Edited by BRANOVER, H.), pp. 255–279. AIAA, Washington, D.C.

LYKOUDIS, P. S. 1989 Private communication.

MICHIYOSHI, I. 1988. Boiling heat transfer in liquid metals. *Appl. Mech. Rev.* **41,** 129–149.

MICHIYOSHI, I., FUNAKAWA, H., KURAMOTO, C., AKITA, Y. & TAKAHASHI, O. 1977 Local properties of vertical mercury–argon two-phase flow in a circular tube under transverse magnetic field. *Int. J. Multiphase Flow* **3,** 445–457.

MICHIYOSHI, I., TANAKA, M. & TAKAHASI, O. 1982 Mercury–argon two-phase heat transfer in vertical annulus under transverse magentic field. *Int. J. Heat Mass Transfer* **25,** 1481–1487.

MICHIYOSHI, I., SERIZAWA, A., TAKAHASHI, O., GAKUHARI, K. & IDA, T. 1986 Heat transfer and hydraulics of liquid metal–gas two-phase magnetohydrodynamic flow. In *Proc. Heat Transfer Conf.*, San Francisco, Calif., Vol. 2, pp. 2391–2396.

MISHIMA, K. & ISHII, M. 1984 Flow regime transition criteria for upward two-phase flow in vertical tubes. *Int. J. Heat Mass Transfer* **27,** 723–737.

OSHIMA, S., YAMANE, R., MOTIMARU, Y. & SUDOU, K. 1985 Investigation of film flow of a conducting fluid in a transverse magnetic field (1st Report, Film flow in a nonuniform magnetic field). *Bull. JSME* **51,** 3471–3479.

PETRICK, M., FABRIS, G., PIERSON, E. S., CURI, D. A., FISCHER, A. K. & JOHNSON, C. E. 1977 Experimental two-phase liquid–metal magnetohydrodynamic generator program. Report ANL/MHD-77-3.

SERIZAWA, A. 1988 Heat transfer of two-phase annular–dispersed flow under a transverse magnetic field. Presented at the *Japan–U.S. Wkshp on Liquid Metal MHD and Related Problems*, Osaka, Japan.

SERIZAWA, A. & KATAOKA, I. 1987 Phase distribution. Presented at *ICHMT Int. Semin. on Transient Phenomena in Multiphase Flow*, Dubrovnik, Yugoslavia.

SERIZAWA, A., TSUDA, K. & MICHIYOSHI, I. 1984 Real-time measurement of two-phase flow turbulence using a dual-sensor anemometry. In *Measuring Techniques in Gas–Liquid Two-phase Flows* (Edited by DELHAYE, J. M. & COGNET, G.), pp. 495–523. Springer, New York.

SERIZAWA, A., GAKUHARI K., IDA, T., TAKAHASHI, O. & MICHIYOSHI, I. 1986a NaK–nitrogen two-phase annular–dispersed flow under a magnetic field. *Proc. 23rd natn. Heat Transfer Symp. Japan* **B324,** 286–288.

SERIZAWA, A., IDA, T., TAKAHASHI, O. & MICHIYOSHI, I. 1986b Flow structure and heat transfer of liquid metal–gas two-phase MHD flow. *JSME Symp. Ser.* **864,** 65–68.

STEEN, D. A. & WALLIS, G. B. 1964 The transition from annular to annular–mist cocurrent two-phase down flow. AEC Report NYO-3114-2.

THOME, R. J. 1964 Effect of a transverse magnetic field on vertical two-phase flow through a rectangular channel. Report ANL-6584.

TOMITA, Y., ISHIBASHI, Y. & SUDOU, K. 1986 A study on the behavior of a ferrofluid jet in a magnetic field (1st Report, Transversely applied magnetic field). *Bull. JSME* **52,** 807–812.

UEDA, T. 1981 *Two-phase Flow* p. 115. Yokendo Publishing, (in Japanese).

VERSHOOR, H. & STEMERDING, S. 1951 Heat transfer in two-phase flow. In *Proc. General Discussion on Heat Transfer*, Section 2. Inst. Mech. Engrs, London.